BARKHAUSEN NOISE: SIMULATIONS, EXPERIMENTS, POWER SPECTRA, AND TWO DIMENSIONAL SCALING

A Dissertation

Presented to the Faculty of the Graduate School

of Cornell University

in Partial Fulfillment of the Requirements for the Degree of

Doctor of Philosophy

by

Matthew Christopher Kuntz

January 2001

Biographical Sketch

Matthew Kuntz was born in California in 1973 to Joel and Karan Kuntz. He grew up in Lake Oswego, Oregon, where he went to Forest Hills Elementary school and Lake Oswego High School. His love of Science began at an early age when he wanted to be a Marine Biologist and study dolphins. His interests were shifted towards Physics by a horrible experience with high-school biology, and two wonderful chemistry and physics teachers.

In 1991, matthew left Lake Oswego to study at Amherst College, in Massachusetts, where he studied Physics, Computer Science, Russian, and anything else he could fit into his schedule. In 1993, he first met his wonderful wife-to-be, Maria Sharikova, who was then a Freshman at Amherst. In 1995, he graduated from Amherst College Summa Cum Laude with a degree in Physics and headed off for Cornell to pursue his Ph.D.

At Cornell, he sweated through all of the introductory courses and began work on Hysteresis (and educational web pages) with Jim Sethna. After four years of work, and hundreds of hours of computer time, Matthew had almost finished his dissertation and was starting to seriously look for jobs when he got a job offer in Boston that he couldn't resist (especially since Maria would be working there, too!). The job started in just three weeks, but he thought he could finish up the dissertation

before he left. Unfortunately (well, perhaps fortunately . . .) as he was creating his last figures, he suddenly figured out the solution to the very first problem he had worked on, which he had long ago given up on! (The results of this accident are documented in chapter 4) His remaining work having suddenly jumped from a days worth to a months worth, he was out of time, so he wrapped up as much as he could and headed off for a new world of professional software development and server-side Java.

At his new job, Matthew was swamped with work, but he continued to work on Hysteresis and finished his dissertation on many late evenings and long weekends. In the midst of all of this, on November 5, 1999, he finally married Maria. Matthew and Maria are living happily together in a cramped appartment in Cambridge. They are eagerly anticipating moving into their first house, in Wellesley, MA, where they will raise their first baby (currently affectionately named "furball"), who will be born in January, 2001.

K MAWE.

Acknowledgements

I would like to thank all of my teachers, who have shared with me not just their knowledge, but their love of learning. Without their enthusiasm and excitement, I never would have survived this far. I would like to thank all of my classmates in my first year at Cornell, without the companionship of whom Quantum Mechanics and Statistical Mechanics would have driven me crazy. I would like to thank the residents of Clark Hall, 5th floor (where I spent most of my time for three years) for their companionship, their ideas, and their feedback. I would like to thank my advisor, Jim Sethna, for all his help, guidance, and enthusiasm. It was Jim's enthusiasm which encouraged me to pursue a study of magnetic hysteresis, and his enthusiasm and constant stream of ideas which kept me going even when nothing seemed to be working. He was great to work with.

Finally, I would like to thank my family. I would like to thank my parents, who always encouraged me in everything I pursued, and always were there to help me, whenever I needed them. I would like to thank my wife, Maria, who has made my life special in so many ways I never imagined possible, and without whom my life would just not be the same.

Portions of this work were supported under NSF DMR-9805422 and DOE DEFG02-88-ER45364. An equipment grant from Intel and the support of the Cornell Theory Center are also gratefully acknowledged.

Table of Contents

1 Introduction **1**

2 Relating the zero temperature RFIM to experiments **4**
2.1 The Models 5
2.2 Pulling the models together 9
2.3 Experiments 19
2.3.1 Front-propagation with strong dipole-dipole interactions . . . 21
2.3.2 Front-propagation with weak dipole-dipole interactions 21
2.3.3 Plain-old critical results 22
2.4 Conclusion 24

3 Scaling of the power spectrum **26**
3.1 Introduction 26
3.2 Deriving the exponents 27
3.2.1 The avalanche shape 28
3.2.2 Distribution of voltages V in avalanches of size S 29
3.2.3 The scaling of avalanche energy E with avalanche size S . . . 32
3.2.4 The scaling of the time-time correlation function with S . . . 32
3.2.5 The scaling of the energy spectrum with S 33
3.2.6 The energy spectrum scaling depends on the large avalanche cutoff 34
3.2.7 The energy at frequency ω scale linearly with the avalanche size S? 36
3.2.8 Integrating the energy spectrum over avalanche sizes 41
3.3 How universal is the exponent $1/\sigma\nu z$? 44
3.4 Discussion 46

4 Scaling in two dimensions **49**
4.1 Scaling the avalanche size distribution in 2D 49
4.2 Is there a problem with nucleation? 55
4.3 Are there symmetry problems? 56
4.4 Is there a problem with the random number generator? 56
4.5 Good scaling at last 57

5 Algorithms for simulating the zero temperature RFIM **60**
5.1 The Brute Force Method 68
5.2 Time Efficiency: Sorted Lists 71
5.3 Space Efficiency: One Bit per Spin 74
5.4 Calculating Histograms and Correlations 79

A The mean field power spectrum **84**

Bibliography **88**

List of Tables

2.1 Important critical exponents for each model. 20

3.1 Exponents related to the power spectrum exponent. 27
3.2 The power spectrum exponent in simulations and theory. 43

List of Figures

2.1 The hysteresis loop of the plain-old-critical model has a jump for $R < R_c$, and is smooth for $R > R_c$. 11
2.2 Critical avalanche size distribution for the plain-old-critical model. . 12
2.3 When infinite range demagnetizing forces are added to the plain-old-critical model, the hysteresis loop is tilted. 13
2.4 The avalanche size distribution near $R = R_c$ is unchanged by the addition of the infinite-range demagnetizing force. 14
2.5 Demagnetizing forces break up the infinite avalanche. 15
2.6 Self organized avalanche size distribution. 16
2.7 The addition of dipole-dipole forces leads to the formation of long, straight, stripe domains along the direction of magnetization. 18

3.1 Typical avalanche shape. 28
3.2 Average avalanche shape. 30
3.3 Voltage distribution collapse 31
3.4 Time-time correlation function collapse. 34
3.5 Energy spectrum collapse for different avalanche sizes. 35
3.6 Scaling with S of the energy spectrum. 36
3.7 The contribution to the energy spectrum from spins at different radii r. 39
3.8 The contribution to the energy spectrum from spins at radius r is independent of avalanche size S. 40
3.9 The power spectrum for the infinite range model. 43
3.10 The energy spectrum of the mean field model. 45
3.11 The energy spectrum for the short range model. 46

4.1 Large disorders collapse well. 50
4.2 No horizontal translations can fix this bump at lower disorders! . . . 51
4.3 The scaling variable s^r gives a good collapse. 52
4.4 At low enough disorders (requiring $45,000 \times 45,000$ simulations!) the scaling becomes bad again. 53

4.5 Between $R = 0.64$ and $R = 0.60$, the correlation length increases drastically, and the hysteresis loops goes from a smooth one to one with most of the system flipped in a single avalanche. This is inconsistent with a critical disorder of $R = 0.38$. It is much more consistent with the critical disorder predicted by the standard scaling form, but this form does not successfully collapse the data near R_c. 54
4.6 Successful 2D scaling 58

5.1 Three dimensional view of avalanche. 64
5.2 Avalanche time series 65
5.3 Avalanche size distributions in three dimensions. 66
5.4 A $30,000 \times 30,000$ simulation with disorder $R = 0.65$, where each pixel represents a 30×30 square, and each avalanche is a different color. Note that there are avalanches of all sizes, with many smaller avalanches, and fewer large ones. 67
5.5 Use of a queue to simulate avalanche propagation 70
5.6 Using a sorted list to find the next spin. 73
5.7 Probabilities of spins flipping. 75
5.8 Running times on 266 MHz Pentium II. 83

A.1 The exact time-time correlation for mean field theory with a maximum time cutoff of $T = 1000$. 87

Chapter 1

Introduction

When an external magnetic field is applied to a ferromagnetic material, several interesting things happen. First, there is hysteresis—the changes in magnetization lag behind the changes in the external field. The most obvious result of this hysteresis is that the material remains magnetized when the external field is removed. Another important effect is called the Barkhausen effect: as the external field is smoothly increased, the magnetization of the material increases not smoothly but in fits and jumps (called avalanches). The noise that is measured when the magnetization changes are measured by a pickup coil is called Barkhausen noise.

This Barkhausen noise exhibits the properties of a critical phenomenon—many aspects of the noise have a power law behavior. The distributions of avalanche sizes, avalanche durations, and avalanche energies are all seen to behave as power laws with apparently universal exponents.[1] Many other properties, such as the power spectrum and the avalanche shapes appear to behave in a universal, critical way.

In recent years, much research has been done on theoretical models of Barkhausen

[1] Actually, several different sets of exponents have been observed in experiments. In chapter 2, I will enumerate them and describe how they can all be explained by a single model exhibiting three different critical behaviors.

noise. In chapter 2, I will review several of these models and compare their results to the results of experiments. The first of these models is called the ABBM model[1], which describes the magnetization of a ferromagnetic material in terms of a single degree of freedom. The more recent models are mostly variations of the random field Ising model (RFIM) at zero temperature.[2, 3, 4, 5, 6, 7, 8, 9, 10] These previous studies have left several open questions which I will discuss in this dissertation.

One aspect of Barkhausen noise which has remained unexplained is how the significant range of exponents observed in experiments can be reconciled with the universal critical exponents predicted by each of the existing models. In chapter 2, I will show that the experimental results fall into three categories, or universality classes. I will then show that the existing models of Barkhausen noise can be unified under one model, which can produce all three categories of exponents depending on the values of tunable parameters. (These tunable parameters correspond roughly to actual properties of the materials being studied in experiments.)

Another aspect of Barkhausen noise which has been been poorly understood theoretically is the power law seen in the power spectrum. This is one of the most commonly measured power laws in experiments, but it has remained largely unexplained by theories of Barkhausen noise. There have been several derivations of this power law[11, 12, 13], but their predictions are not only completely inconsistent with the results observed in experiments, but also completely inconsistent with simulations of the theoretical models they purportedly apply to. In chapter 3, I will show how these previous derivations were wrong and derive a new prediction of the power spectrum exponent which produces very good agreement with both simulations and experiments.

The characteristics of Barkhausen noise in two dimensions have been a persistent

source of confusion. Two dimensional simulations definitely appear to exhibit power laws indicative of critical behavior. However, when rigorous attempts have been made to understand these power laws in terms of critical phenomena, the results have been inconclusive. I have run very large simulations in attempts to understand this behavior. Rather than solving the problems, these large simulations have made even more obvious the problems with the scaling of Barkhausen noise in two dimensions. I will describe the current results on two dimensional scaling in chapter 4.

In order to run the very large simulations (up to two billion Ising spins) necessary to properly study our models of Barkhausen noise, we have needed to develop sophisticated algorithms for simulation. In chapter 5, I will describe in detail each of the algorithms we have used. The most sophisticated of these algorithms uses only one bit of memory per spin (in addition to a constant overhead which does not scale with the number of spins) and has an $O(N \log N)$ running time. A simulation of two billion spins will run in less than a day.

Chapter 2

Relating the zero temperature RFIM to experiments

In experiments, many measured properties of Barkhausen noise follow power laws. One of the first power laws observed in Barkhausen noise is the behavior of the power spectrum at high frequencies.[1] Recently, as experimental techniques have improved, it has become possible to distinguish individual jumps, or avalanches, in the Barkhausen noise. Many properties of these avalanches also obey power laws. These properties include the distribution of avalanche durations, the distribution of avalanche sizes, the distribution of avalanche energies, and the relationship between avalanche duration and avalanche size.

Inspired by the link between thermally driven critical points, scale invariance, and power laws, several groups have recently tried to explain the characteristics of Barkhausen noise in terms of either a disorder driven critical point or disorder driven self-organized criticality.

[1]The power spectrum at high frequencies is determined by the internal structure of avalanches, as well as the distribution of avalanche sizes. The low frequency power spectrum is determined by the spacing between avalanches and has a different behavior. (See chapter 3)

2.1 The Models

There are two primary processes involved in Barkhausen noise. The first process is domain nucleation. Early in the magnetization process and late in the magnetization process, when there are few domains, domain nucleation is the dominant source of Barkhausen noise. Unless there is very strong disorder (which makes domain nucleation very easy), once domains become well established the motion of existing domain walls becomes the dominant magnetization process.

Because domain wall motion is thought to be the most important process during most of the magnetization process, many researchers have focused on understanding domain wall motion in order to understand Barkhausen noise. Many experiments have focused on materials in which dipole-dipole interactions cause long smooth domains to form parallel to the magnetization. In these materials, nucleation is almost non-existent once the domains are formed.

To explain the properties of the Barkhausen noise observed in these materials, Alessandro et. al.[1] proposed a simple model (called the ABBM model, after its inventors) of domain wall motion. They based their model on two observations. First, because the domain wall is long and smooth, domain wall motion can be characterized by one parameter: the thickness of the domain. Second, it was observed that the coercive field measured in experiments was a random function of the width of the domain wall, approximately described by a Wiener-Lévy stochastic process. They combined these two observations with equations for the magnetostatic interactions to produce a single degree-of-freedom (domain wall width) model of Barkhausen noise.

The ABBM model has turned out to be extremely successful in predicting the exponents of the power laws in Barkhausen noise in certain classes of materials.

However, it leaves an important question unanswered: why is the coercive field described by a Wiener-Lévy stochastic process? If it were not, then the ABBM model would predict different power laws, or no power laws at all. One of the first hypotheses was that the defects and disorder in the material are correlated. However, experiments have shown that the correlation length of the defects in materials is much shorter than the correlation length needed to make the ABBM model work.

Another possible solution to this problem is that the power-law behavior of Barkhausen noise arises not from the spatial distribution of the disorder, but from the collective action of many degrees of freedom. In particular, collective action could lead to critical behavior, a natural source of power laws. In this case, the power laws would be universal, and independent of the particular spatial distribution of disorder.

For ferromagnetic systems, a natural model of collective behavior is the Ising model. Because the systems of interest are far from equilibrium, it makes sense to model the systems at zero temperature. The quenched disorder in the materials can be modeled by random fields, random bonds, or a diluted lattice. It has been argued that at zero temperature, the random field, random bond, and diluted Ising models all fall in the same universality class. ([11]) The random field Ising model is the easiest to simulate, and several variations have been proposed as explanations of Barkhausen noise. These models have all had significant success explaining properties of Barkhausen noise in various experiments. (But different models have had success explaining different experiments.)

In 1992, Ji and Robbins[7] proposed a simple model of domain wall motion based

on the RFIM. They proposed a simple Hamiltonian:

$$\mathcal{H} = -\sum_{\text{nn}} s_i s_j - \sum_i (H + h_i) s_i, \tag{2.1}$$

where s_i is an Ising spin (± 1), h_i is a random field[2], and H is an external magnetic field. In order to model domain wall propagation, they proposed a simple dynamics: a spin will flip over when it becomes energetically favorable for it to do so, *if* it has at least one neighbor up. The condition that one neighbor must be up for a spin to flip eliminates all domain nucleation, producing a front propagation model. Depending on the strength of the disorder, Ji and Robbins found that there were three different behaviors. For weak disorder, they found a simple faceted growth. For intermediate disorder, they found a compact, self-affine growth. For high disorder, they found a fractal, self-similar growth. In all three regimes, there was a value of $H = H_c$ at which the domain wall depinned and spanned the system. In the self-affine and self-similar regimes, the approach to H_c was critical, and there was a power law distribution of avalanche sizes and durations. The self-similar growth is less likely to be observed in ferromagnetic materials, because at disorders large enough to produce self-similar growth, domain nucleation is likely to be a dominant process. Narayan and Fisher[9] did an epsilon expansion for the critical exponents of this model in the self-affine regime.

Although domain wall motion is thought to be the primary source of Barkhausen noise, in real materials domain nucleation is present, and there are multiple interacting domains. To capture these features, Sethna et. al. proposed extending Robbins' model to include domain nucleation. They did this by changing the dynamics so that spins can flip even when all of their neighbors are unflipped. For low disorders, domain nucleation remains unimportant, and there is still self-affine domain wall

[2]Many different distributions of random fields are possible, but identical, universal power laws occur for a wide range of distributions.

growth with a depinning transition at a particular $H = H_c$. However, at larger disorders, there is a second-order critical point, at which domain nucleation eliminates the depinning transition and produces a macroscopically smooth magnetization process. At this critical point, there is a power law distribution of avalanche sizes and durations, with a new set of critical exponents. This critical point was observed to have a very wide critical region, so it is expected that experiments with high disorder might observe these critical exponents even without tuning the disorder.

Both Robbins' and Sethna's models ignored the presence of long-range forces. In experiments, long-range forces have been observed to play an important role.[8, 14] The primary source of long-range interactions in ferromagnetic materials is the dipole-dipole interaction between spins. In some materials, these interactions are very week in comparison to the short-range exchange interactions, and can possibly be ignored. In other materials, they have a strong effect, and cause the material to form long domains parallel to the direction of the magnetization.

In 1995, Urbach et. al.[10] proposed that rather than being coincidentally close to a critical point, experimental systems are self-organized to a critical point by the long-range forces. Specifically, they added an infinite range demagnetizing field to a two-dimensional front-propagation model similar to the model of Ji and Robbins'. This demagnetizing force is not as unrealistic as it might seem at first glance. Real experimental samples, however large, are finite in size, and everywhere a domain crosses the boundary of the system the dipole-dipole interactions produce an effective long-range demagnetizing force. Except in special experimental geometries, where the domain walls do not cross the sample boundary, this demagnetizing force has been observed to have a significant effect on experiments.

Urbach et. al. found that the demagnetizing force indeed self-organized their

model. When the domain wall tried to depin, the demagnetizing force grew until it stopped the domain wall, and returned the system to the depinning transition. Over a wide range of external fields power-law distributions were observed, with the same exponents as the distributions at the depinning transition in the short-range model. Narayan[9] performed a more rigorous theoretical justification for this self-organization.

Cizeau, Zapperi, Durin and Stanley[8, 14] further examined this problem. They considered a continuum version of Urbach's model with full dipole-dipole interactions added. (They retained an infinite-range demagnetizing force as an approximation of the boundary effects, since they appear to play an important role in experiments.) Like Urbach et. al., they found that the demagnetizing force self-organized the system. However, they also showed that the dipole interactions lowered the upper critical dimension of the system from five to three, leading to mean-field behavior. In addition, they showed that this mean-field behavior produced the same exponents as the single-degree-of-freedom ABBM model. This finding resolved one of the major questions raised by the ABBM model: the correlated pinning field needed for the ABBM model arises not from a particular spatial distribution of disorder, but from the collective action of an extended interface.

2.2 Pulling the models together

The models above produce three different sets of critical exponents—three dimensional front propagation (Ji and Robbins and Zapperi et. al. without dipole), plain old critical (Sethna et. al.), and mean field (Zapperi et. al., with dipole). However, each of the models left out important aspects of real physical systems. The models of Ji and Robbins, Urbach, and Zapperi et. al. all left out both domain nucleation

and interactions between domains. On the other hand, the model of Sethna et. al. completely ignored the effects of long-range interactions. The question arises—will multi-domain interactions, domain nucleation, and long range forces interact with each other to produce a new type of behavior.

To examine this possibility, we have recently extended the plain old critical model (short range interactions with domain nucleation) to include both demagnetizing and dipole forces. The Hamiltonian for this model (which can be used for all of the mentioned models, by setting appropriate constants to zero, and enforcing the appropriate dynamics) is

$$\begin{aligned}\mathcal{H} = &- \sum_{nn} J_{\mathrm{nn}} s_i s_j - \sum_i (H + h_i) s_i \\ &+ \sum_i \frac{J_{\mathrm{inf}}}{N} s_i - \sum_{\{i,j\}} J_{\mathrm{dipole}} \frac{3\cos(\theta_{ij}) - 1}{r_{ij}^3} s_i s_j,\end{aligned} \tag{2.2}$$

where J_{nn} is the strength of the nearest neighbor interactions, J_{inf} is the strength of the infinite range demagnetizing force, J_{dipole} is the strength of the dipole-dipole interactions, θ_{ij} is the angle between the line joining s_i to s_j and the direction of magnetization, and r_{ij} is the distance between s_i and s_j. In this section, we will consider the dynamics previously used by Sethna et. al., which include domain nucleation.

The simplest version of this model is the original model of Sethna et. al.. This case arises when both J_{inf} and J_{dipole} are set to zero. As can be seen in figure 2.1, there is a phase transition from hysteresis loops with a finite jump (we will call this jump an infinite avalanche from now on—in the thermodynamic limit, it involves infinitely many spins) to macroscopically smooth hysteresis loops. At this transition, there is a critical distribution of avalanche sizes, durations, energies, and other properties. The distribution of avalanche sizes near the critical point can be

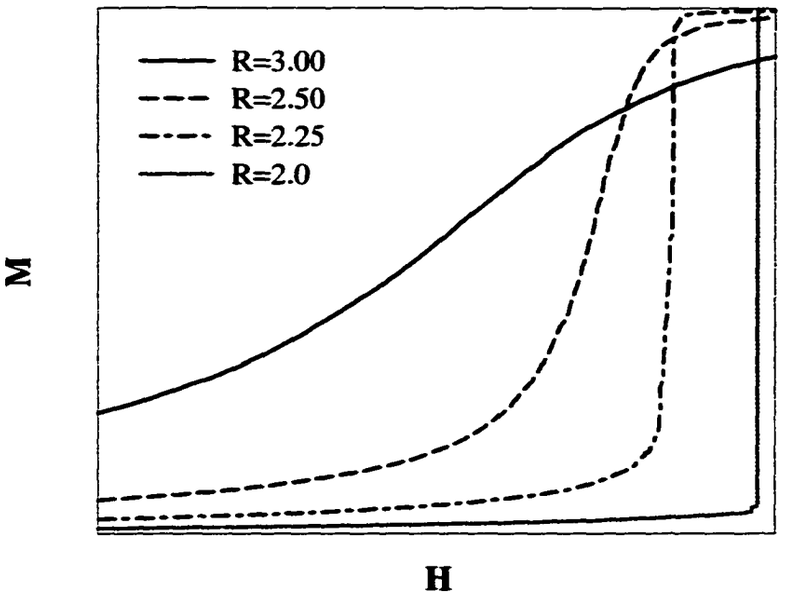

Figure 2.1: The hysteresis loop of the plain-old-critical model has a jump for $R < R_c$, and is smooth for $R > R_c$.

seen in figure 2.2.

The effect of adding infinite range demagnetizing forces to this model depends on the disorder. First, let us consider what happens at high disorders where there is no infinite avalanche. As defined in equation 2.2, the strength of the demagnetizing field decreases in proportion to the size of the system. This is actually a realistic definition—in real materials the demagnetizing forces result from boundary effects which become weaker and weaker as the size of the sample grows. This means that in the thermodynamic limit, only avalanches which occupy a finite fraction of the system will cause a finite change in the demagnetizing force. Because of this, the non-infinite avalanches at large disorder will be unaffected by the addition of a demagnetizing force. The only effect of the demagnetizing force will be to increase the magnetic field required to start each avalanche (an avalanche that would start at a field H without the demagnetizing field will start at a field of $H + MJ_{\text{inf}}/N$ in the

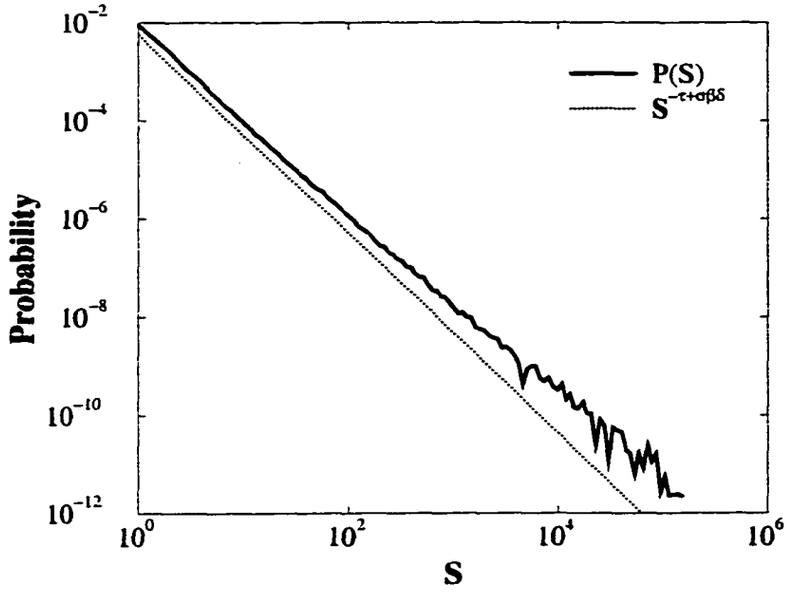

Figure 2.2: The avalanche size distribution for the plain-old-critical model at $R \sim R_c$ (integrated over all values of H) has a power-law distribution, which decays with an exponent $\tau + \sigma\beta\delta \sim 2$. The divergence from a simple power law decay is a result of being slightly above R_c, instead of at the critical point. At $H = H_c$, the (unintegrated) avalanche size distribution decays with an exponent of $\tau \sim 1.6$.

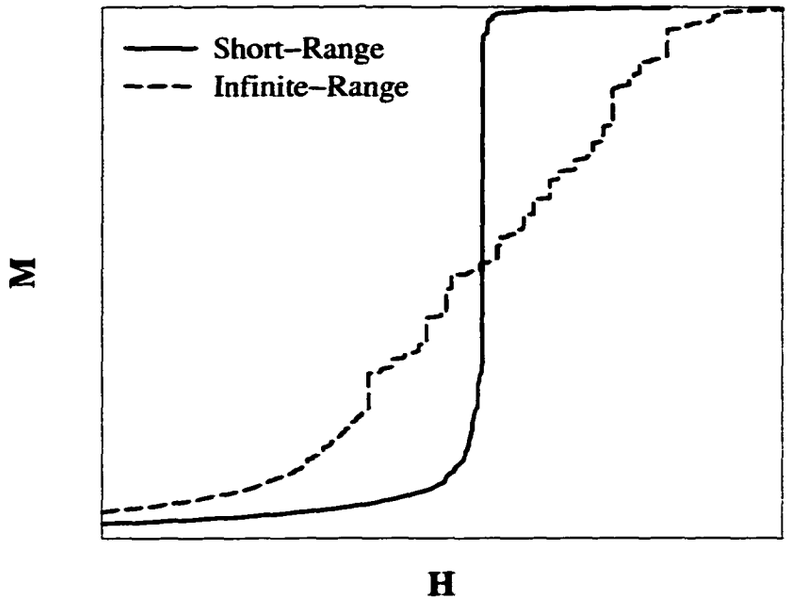

Figure 2.3: When infinite range demagnetizing forces are added to the plain-old-critical model, the hysteresis loop is tilted.

presence of the demagnetizing field), and thus to tilt the hysteresis loop. The tilt in the hysteresis loop can be seen in figure 2.3. As can be seen in figure 2.4, the critical distribution of avalanche sizes is unchanged—even in the presence of demagnetizing forces, the scaling behavior near the second order critical point should be visible in experiments with large enough disorder.

For small disorders $R < R_c$, the effect of demagnetizing forces is much more important. At these disorders, in the absence of demagnetizing forces, there is an infinite avalanche which occupies a finite fraction of the system, even in the thermodynamic limit. Hence, even in the thermodynamic limit, this avalanche will cause a finite increase in the demagnetizing field. As the demagnetizing field increases, the effective field felt by the avalanche decreases below the field necessary for the avalanche to continue propagating, and the avalanche halts until the external field is increased again. This process breaks up the infinite avalanche into many smaller

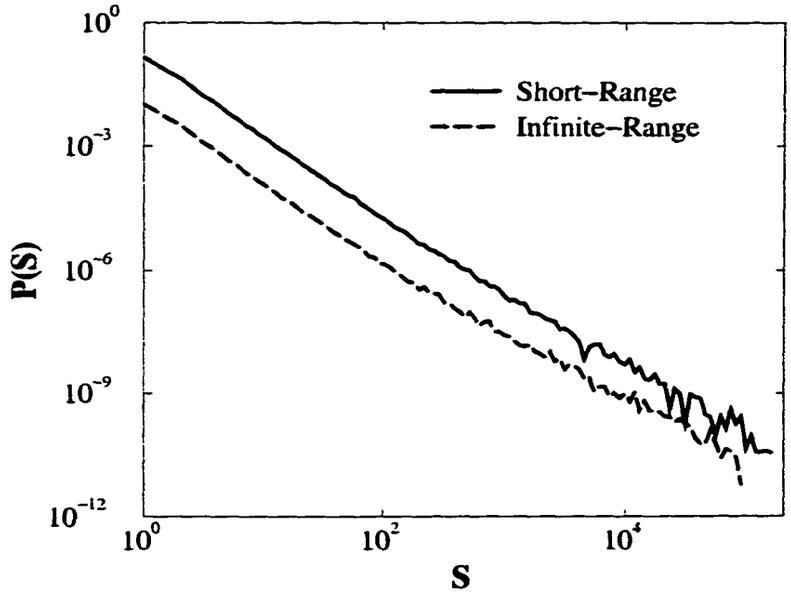

Figure 2.4: The avalanche size distribution near $R = R_c$ is unchanged by the addition of the infinite-range demagnetizing force.

avalanches with a critical distribution of sizes. The infinite avalanche becomes a propagating front. Because there are few clusters of preflipped spins ahead of the avalanche for disorders $R < R_c$, and these clusters are small, the propagating front has the same properties as the fronts modeled by Ji and Robbins, by Urbach et. al., and by Cizeau et. al.. As Cizeau et. al. found for the front propagation model, the front is self-organized by the demagnetizing field. The hysteresis loop for this situation can be seen in figure 2.5. The avalanche size distribution can be seen in figure 2.4. Note that it has a different scaling exponent than the distribution at the second order critical point.

Even below R_c, the small avalanches before and after the infinite avalanche are unaffected by the demagnetizing field, and their behavior continues to be influenced by the nearby second order critical point. In fact, if one measured the critical behavior over the entire hysteresis loop, and not just within the infinite avalanche,

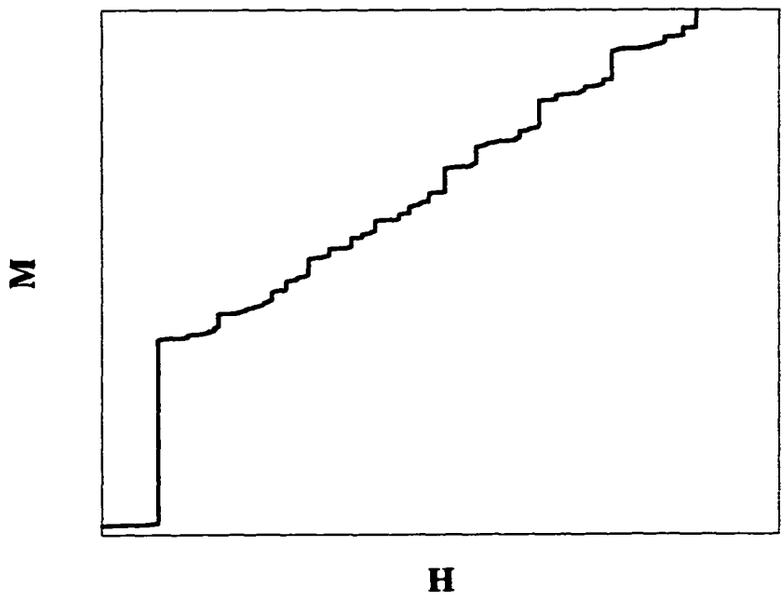

Figure 2.5: For $R < R_c$, the infinite avalanche is broken up by the demagnetizing forces and the vertical part of the hysteresis loop becomes tilted with a constant slope. The initial jump in M is presumably a nucleation effect, and would get smaller gradually as the system size was increased.

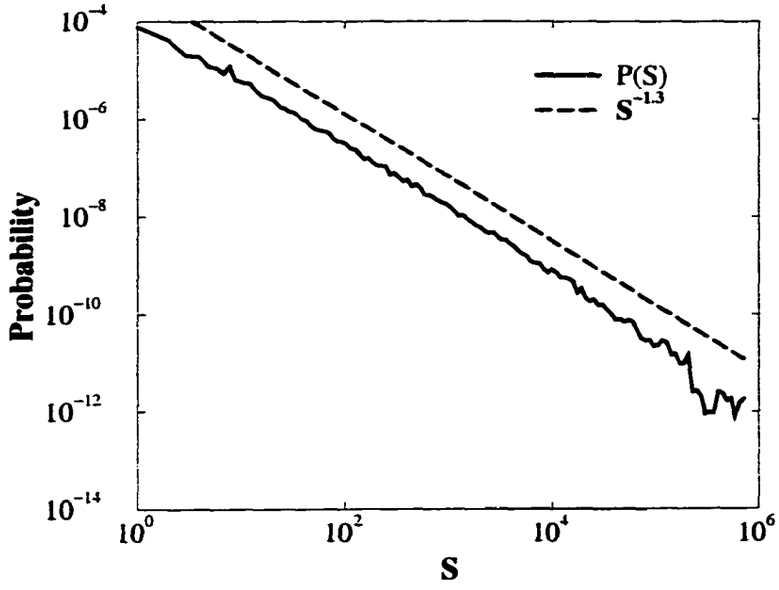

Figure 2.6: For $R < R_c$, the demagnetizing forces self-organize the system to a critical front-propagation behavior. The avalanche size distribution decays as a power law with an exponent $\tau = 1.3$, as for non-self-organized front-propagation. The presence of domain-nucleation does not change the exponent. Notice that because it is self-organized, the system is right at the critical point and there are six decades of scaling with no tuning of parameters. There are also no signs of corrections to scaling from being away from the critical point.

one would find a crossover between the front-propagation exponents and the second order critical exponents as $R \to R_c$. However, this crossover would be seen only in a very narrow range of R—one does not have to go very far below R_c in two and three dimensions before the infinite avalanche takes up most of the system and all remnants of the second order critical point are washed out.

Since, for small R, the addition of demagnetizing forces leads to front-propagation behavior, one would expect that the addition of dipole forces would have the same effect as was described by Cizeau et. al. for the front-propagation models. Indeed, this seems to be the case. The addition of dipole forces leads to the formation of long domains in the direction of magnetization, just as seen in experiments. (see figure 2.7) In our simulations with dipole forces, the results seem consistent with the mean field results claimed by Cizeau et. al. However, since the addition of domain nucleation requires us to model the entire bulk of the material, and not just the domain surface[3], the addition of dipole-dipole interactions is much more computationally costly in our model, and we have not been able to run large enough systems to check this well.

Though their strength relative to the exchange interactions varies dramatically, dipole-dipole interactions are *always* present in ferromagnetic materials. The question arises, can either the simple front-propagation behavior or the plain-old-critical behavior survive the addition of weak enough dipole interactions. It seems likely that in a large enough system any dipole interactions, however weak, would change the universality of either the front-propagation or the plain-old-critical behavior. Not only do the dipole interactions add a long-range interaction, but they add a preferred direction to the Hamiltonian. In the case of the front-propagation crit-

[3]With the front-propagation dynamics of Cizeau et. al., which allows no overhangs, it is possible to model just the surface.

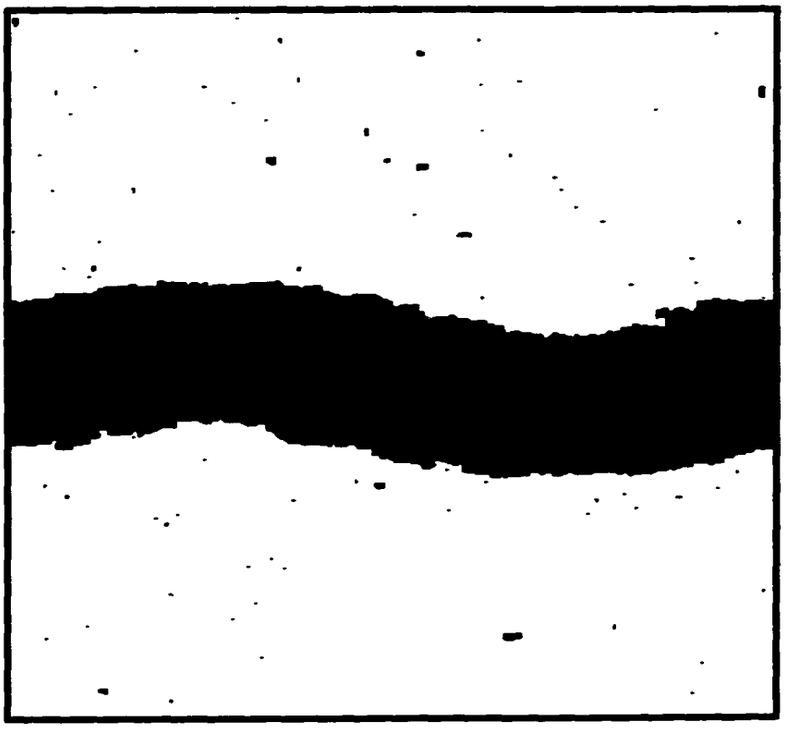

Figure 2.7: The addition of dipole-dipole forces leads to the formation of long, straight, stripe domains along the direction of magnetization.

ical behavior, this has the effect of lowering the upper critical dimension to three and producing mean field exponents. It is likely that it also produces a new second order critical point with new exponents. However, for finite systems, and weak enough dipole interactions, the dipole-free critical behavior seems to persist. Not only do very weak dipole interactions not seem to effect our small simulations, but, as will be described in the next section, experiments appear to have measured both front-propagation and plain-old-critical scaling.

2.3 Experiments

As we showed in the previous section, one model can produce the results seen by the ABBM single degree of freedom model, the simple front-propagation model described by Ji and Robbins, the SOC front-propagation model described by Urbach et. al. and Cizeau et. al. (this SOC model has the same exponents as the non-SOC model of Ji and Robins), the front-propagation model with dipole-dipole interactions described by Cizeau et. al. (which has mean-field exponents), and the second order critical behavior described by Sethna et. al..

In all, there are three different sets of critical exponents (for a three-dimensional lattice) which can arise from this model, depending on the relative strengths of the forces in the material, and the degree of disorder. (See table 2.1) One wonders which (if any) of these behaviors are seen in real experiments. One also wonders whether one can look at the properties of the experimental materials and guess which critical behavior will be observed.

Table 2.1: The exponents from all the models described in this paper fall into three universality classes. The exponents in three dimensions are shown in this table. τ is the exponent describing the distribution of avalanche sizes. $(\tau-1)/\sigma\nu z+1$ is the exponent describing the distribution of avalanche durations. $(\tau-1)/(2-\sigma\nu z)+1$ is the exponent describing the distribution of avalanche energies. $1/\sigma\nu z$ is the exponent describing the high frequency power spectrum. The derivation of this exponent can be found in chapter 3. The plain-old-critical exponents describe the behavior of the short-range model with domain nucleation at $R = R_c$ and $H = H_c$. The front-propagation exponents describe the SOC behavior when infinite range demagnetizing fields are added to either the short-range front propagation model, or the short-range domain nucleation model at $R < R_c$. The mean-field exponents are seen when dipole-dipole interactions are added to a SOC front-propagation model, and also in the single degree of freedom ABBM model.

	τ	$\frac{\tau-1}{\sigma\nu z}+1$	$\frac{\tau-1}{2-\sigma\nu z}+1$	$1/\sigma\nu z$
Plain-Old-Critical	1.6	2.05	1.42	1.72
Front-Propagation	1.3	1.51	1.21176	1.71
Mean-Field	1.5	2.0	1.33	2.0

2.3.1 Front-propagation with strong dipole-dipole interactions

Because of the focus on domain wall motion in understanding Barkhausen noise, many experiments have focused on studying materials with very simple domain structures—one or a few long domains spanning the sample in the direction of magnetization. These long simple domains are a result of strong dipole-dipole interactions (or, equivilently, weak exchange interactions) and fairly small disorder. Therefore, according to this model, and the results of Cizeau et. al., one would expect these materials to produce mean-field exponents. Indeed, this seems to be the case!

Zapperi et. al.[14] describe the results of experiments in $Fe_{21}Co_{64}B_{15}$ amorphous alloy. They show a picture of the domain structure in their sample which looks remarkably like the domain structure depicted in figure 2.7. In their experiments, they measure the exponents $\tau = 1.5$ and $(\tau - 1)/\sigma\nu z + 1 = 2.0$, as one would expect in mean-field theory.

Earlier, Grosse-Nobis[15] studied the motion of a single domain wall in a single-crystal silicon-iron alloy. He used a frame geometry to minimize the effects of demagnetizing fields. As in the experiments of Zapperi et. al., there was a simple domain wall extending across the sample in the direction of magnetization. Grosse-Nobis measured the power spectrum, and found that it had a $1/\omega^2$ decay, as predicted by mean field theory.

2.3.2 Front-propagation with weak dipole-dipole interactions

Not all experiments have been performed on materials with simple dipole-induced domain structures. Urbach et. al.[10] measured avalanche size distributions in a

sample of Fe-Ni-Co alloy. Because they wanted well separated Barkhausen pulses, they prepared the sample to have particularly strong pinning. As a side effect, the dipole-dipole interactions were relatively less important. In this material, Urbach measured a value of $\tau = 1.33$, which agrees well with the dipole-free self-organized front-propagation exponent.

Durin and Zapperi[16] performed experiments in which they tried to further explore the transition between front-propagation and mean-field behavior. They studied samples of $Fe_{64}Co_{21}B_{15}$ in which the importance of short-range interactions relative to the long-range dipole interactions was increased with the addition of tensile stress. They measured both the avalanche size distribution and the avalanche duration distribution with the sample under tensile stress, and found exponents of $\tau = 1.3$ and $(\tau - 1)/\sigma\nu z + 1 = 1.5$, in excellent agreement with the dipole-free front propagation exponents.

2.3.3 Plain-old critical results

Other experiments have produced results which seem to fit well with the plain-old critical model. Many of these experiments have attempted to fit their data with the ABBM model. One such case is the experiments of Alessandro et. al. (the creators of the ABBM model). Alessandro et. al.[17] performed experiments on non-oriented polycrystalline SiFe alloys. Because of their non-oriented polycrystalline nature, we might expect both dipole and demagnetizing forces to play a much smaller role. (The preferred direction of the dipole forces is different in different crystals, except when the sample is very strongly magnetized.) Moreover, the polycrystalline sample is likely to have an effectively higher disorder, so it is likely that we might see the behavior of the second-order critical point, rather than the lower disorder front-

propagation behavior.

Although Alessandro et. al. fit their power spectra with some success using the ABBM model, most of their experimental curves appear to have a slower high frequency decay than the ω^{-2} which they fit to. In fact, attempting to read the exponent off their graphs (they don't actually try to fit the exponent of the decay), it appears that they measured a power spectrum with an exponent of ~ 1.6. This is much more consistent with the front-propagation exponents or the second-order-critical exponents than it is with the mean-field/ABBM exponents.

In a later paper, Bertotti et. al.[18] reported measurements of avalanche statistics in a similar polycrystalline SiFe sample. They claimed to measure an avalanche size distribution exponent of $\tau = 1.5 - c/2$, where c is a measure of the driving rate.[4] Indeed, their measurements fit this form for large driving rates c. However, their measurements at *small* c deviate from this form. Their measured exponent for the slowest driving was approximately $\tau = 1.63$. This is significantly higher than the maximum of $\tau = 1.5$ expected from the ABBM model or mean-field theory. In fact, it is in very good agreement with the value $\tau = 1.6$ predicted by the plain-old-critical model. Taken with the power spectra measured by Allesandro et. al.[17], this seems to indicate that plain-old-critical behavior can be observed in non-oriented polycrystalline samples.

Another experiment which appears to have plain-old-critical exponents is the experiment described by Spasojević et. al.[12]. Spasojević et. al. measured many properties of avalanches in a commercial VITROVAC 6025 X metal glass sample. They measured exponents of $\tau = 1.77$, $(\tau-1)/\sigma\nu z+1 = 2.22$, $(\tau-1)/(2-\sigma\nu z)+1 = 1.56$, and $1/\sigma\nu z = 1.6$. These results are all quite close to the results predicted by the

[4] At high driving rates, small avalanches overlap, creating more large avalanches and fewer small avalanches. This leads to a decreased scaling exponent.

plain-old-critical model. (and completely inconsistent with the other two models) Except for $1/\sigma\nu z$, each of the exponents seems to be a little bit high. This is what the plain-old-critical model would predict if they measured Barkhausen pulses over slightly too wide a range of H. If they measured over the entire hysteresis loop, then $\tau = 1.6$ would be replaced everywhere by $\tau + \sigma\beta\delta = 2.03$.

2.4 Conclusion

Theoretical models of Barkhausen noise seem to fall into one of three universality classes. By varying the relative strengths of parameters, all three of these behaviors can be produced by a single model based on the random-field Ising model. This model includes the effects of both domain-motion and domain-nucleation, along with both demagnetizing and dipole fields. The three universality classes produced by this model seem to be capable of describing a large set of experiments, the results of which previously seemed incompatible.

When the disorder is low, and dipole interactions are strong, this model produces mean-field results. These results are the same as the results of the single degree of freedom ABBM model. Many experiments have been performed on soft magnetic materials, in which the disorder is fairly low, and dipole interactions lead to long parallel domains in the direction of magnetization. In these samples, the properties of the Barkhausen pulses seem to be well described by the mean-field exponents.

When the dipole interactions are weaker, the model produces non-mean-field front-propagation exponents. The system is self-organized by the presence of demagnetizing fields. In experiments with somewhat stronger disorder, or stronger exchange interactions, these exponents have been observed.

For high enough disorder and weak enough dipole interactions, the model pro-

duces critical distributions of avalanche properties due to proximity to a disorder-induced second order critical point. These exponents have been observed in experiments on polycrystalline samples, where the disorder is high, and the effects of dipole-dipole interactions are reduced by the lack of a well-defined orientation.

Other effects can modify the exponents observed in experiments. All of the predictions of this model assume an infinitesimal driving rate. If the external field in experiments is ramped up too quickly, avalanches will overlap, leading to more large avalanches, fewer small avalanches, and decreased exponents. Also, experiments must be careful to measure Barkhausen noise only in the steepest part of the hysteresis loop. (Except for high disorder systems near the second-order critical point, experiments are likely to be self-organized, and this should be quite a large region of the hysteresis loop.) At the extremities of the hysteresis loop, there are fewer large avalanches, and the measured exponents will be higher.

Chapter 3

Scaling of the power spectrum

3.1 Introduction

One of the main power laws which must be explained if our theoretical models are to be successful is the power law behavior of the power spectrum. Actually, the power spectrum exhibits two different power laws, one for low frequencies, and another for high frequencies. The high frequency power law, $\mathcal{P}_{\rm av}(\omega)$, reflects the dynamics within avalanches, and the low frequency power law, $\mathcal{P}_{\rm corr}(\omega)$, reflects the correlations between avalanches. Simulations of the various random field Ising models have been fairly successful in modeling the high frequency scaling of the power spectrum, but theoretical predictions of this scaling have been absent or wrong.[3, 6, 11, 8] (See the discussion in section 3.4 for a description of several previous calculations.) In this chapter, I will derive an exponent relation for the high frequency power spectrum which applies to all of the models described in chapter 2. Large portions of the derivation should also apply to any critical avalanche model.

In this derivation, I will relate the power spectrum power law to two exponents: τ, the exponent describing the distribution of avalanche sizes, and $\sigma\nu z$, the exponent

Table 3.1: Important exponents for the three universality classes. τ is the exponent for the avalanche size distribution $D(S) = S^{-\tau}$. $\sigma\nu z$ relates the avalanche size S to the avalanche duration T : $T \sim S^{\sigma\nu z}$

	Short Range (3D)	Front Propagation (3D)	Mean Field
τ	1.6	1.28	1.5
$\sigma\nu z$	0.58	0.58	0.5
	Short Range (4D)	Front Propagation (4D)	
τ	1.53	1.42	
$\sigma\nu z$	0.52	0.56	

describing the relationship between avalanche size and avalanche duration. The values of these exponents for each of the models described in chapter 2 are given in table 2.1. Except in section 3.3, all of the results in this paper are from three-dimensional simulations with nearest neighbor and infinite range interactions, which exhibit self-organized front-propagation exponents.

3.2 Deriving the exponents

In the process of deriving the form of the critical exponent for the energy spectrum, we will derive the scaling forms of several other quantities which are themselves of interest. Warned by the failure of the naive scaling exponent for the energy spectrum, we will present numerical scaling plots for each of these intermediate quantities.

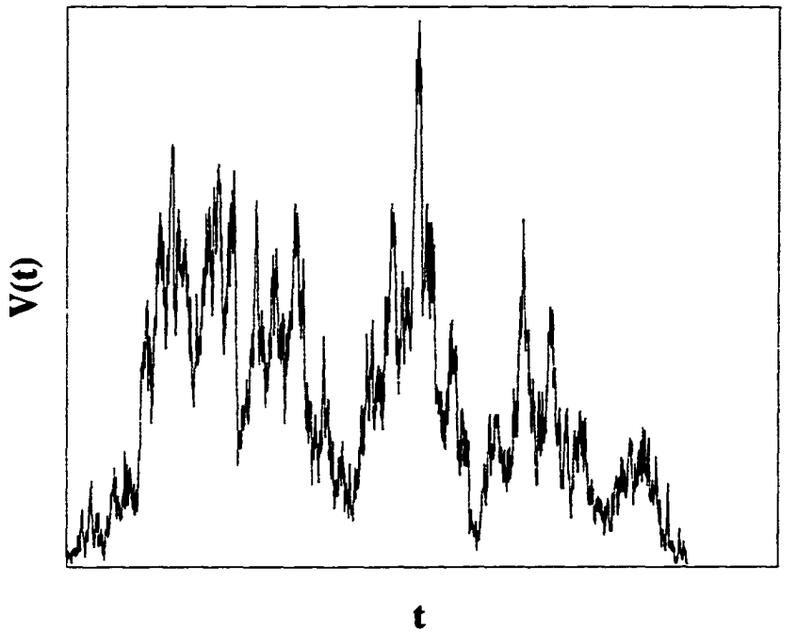

Figure 3.1: The shape of a typical large avalanche. Notice that the avalanche nearly stopped several times, and the voltage (the number of spins flipped in each time step) fluctuated drastically.

3.2.1 The avalanche shape

Near criticality, the avalanches in the random-field Ising model have a very ragged shape. There are avalanches of all sizes precisely because each avalanche is always finely balanced between continuing and dying out. Most large avalanches come close to dying many times. A typical large avalanche can be seen in figure 3.1.

Despite this rough shape, criticality implies that the average avalanche shape will scale in a universal way. Consider the average shape of avalanches of duration T. If we rescale the time axis, t, by a factor of T, and divide the vertical axis, which measures the number of spins flipped (or the voltage V which would be measured in a pickup coil), by the average voltage, we should get a generic shape which is independent of T. The average height is the average area, $S(T) \sim T^{1/\sigma\nu z}$ (let this

define the exponent $\sigma\nu z$)[1], divided by the duration, T. Therefore, the scaling form should be

$$V(T,t) = T^{1/\sigma\nu z - 1} f(t/T). \tag{3.1}$$

The scaling of the average avalanche shape according to equation 3.1 can be seen in figure 3.2.[2]

3.2.2 Distribution of voltages V in avalanches of size S

The power spectrum is sensitive not only to the shapes of the avalanches, but to the fluctuations in the avalanche shapes. An interesting measure of these fluctuations is the probability $P(V|S)$ that a voltage V will occur at some point in an avalanche of size S. If this probability scales universally, then we know it must have the form

$$P(V|S) = V^{-x} f(VS^{-y}). \tag{3.2}$$

But what are the exponents x and y? We can determine the value of x by integrating over all voltages. Since $P(V|S)$ is a probability distribution, it must integrate to 1:

$$\int_0^\infty V^{-x} f(VS^{-y}) dV = AS^{-y(x-1)} = 1. \tag{3.3}$$

From this, we know that $x = 1$. (The alternative, $y = 0$, can be discarded because along with equation 3.2 it would imply that $P(V|S)$ is independent of the avalanche size S.)

[1] In earlier papers[2, 3, 4, 5, 6], our group has called the exponent relating avalanche size to avalanche duration $\sigma\nu z$. σ is the exponent describing the growth of the cutoff in the avalanche size distribution with increasing disorder. ν is the exponent describing the growth of the correlation function as the critical disorder is approached. z describes the dynamics of the model.

[2] This shape is very well fit by an inverted parabola. In mean field theory, this fit seems to be exact.

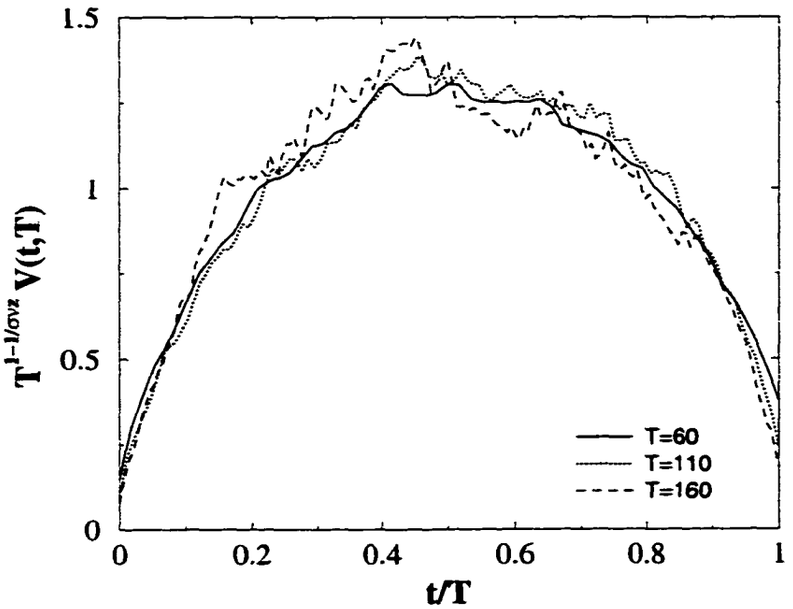

Figure 3.2: The average avalanche shape for three different durations. Spasojević *et al.*[8] measured the average avalanche shape experimentally and found a somewhat different shape. This kind of measurement provides a much sharper test for the theory than the tradition of comparing critical exponents. Presumably, the average avalanche shape for large sizes and times is a universal scaling function: if the experiment differs in this regard from our model, then our model is expected to have different critical exponents. All features at long length and time scales should be universal.

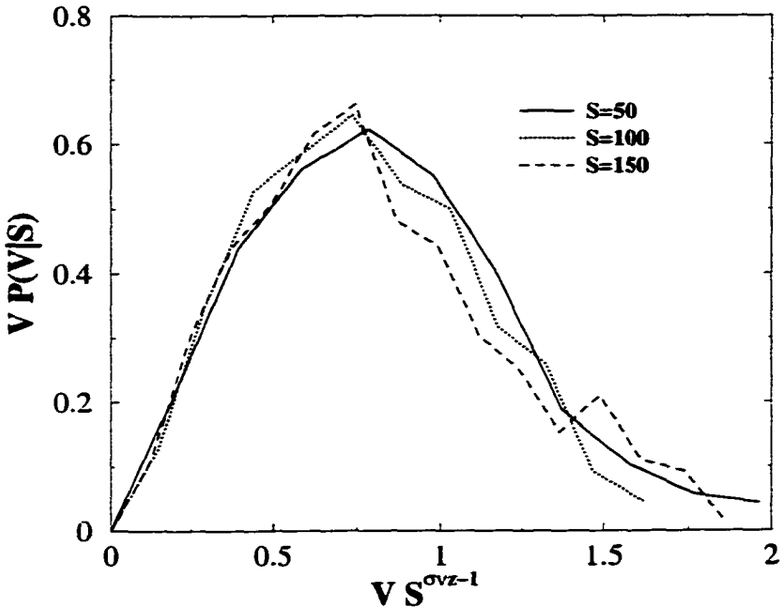

Figure 3.3: A collapse of the voltage distribution for three avalanche sizes according to equation 3.5.

We also know that the average voltage in the avalanche must be equal to the avalanche size S divided by the avalanche duration $T \sim S^{\sigma\nu z}$, so

$$\begin{aligned} \langle V \rangle &= \int_0^\infty V P(V|S) dV \\ &= \int_0^\infty f(VS^{-y}) dV \\ &\sim S^y \sim S^{1-\sigma\nu z}. \end{aligned} \tag{3.4}$$

From this, we know that $y = 1 - \sigma\nu z$, and the probability of a voltage V occurring in an avalanche of size S is

$$P(V|S) = V^{-1} f(VS^{\sigma\nu z - 1}). \tag{3.5}$$

As can be seen in figure 3.3, this scaling form works very well.

3.2.3 The scaling of avalanche energy E with avalanche size S

The voltage distribution in equation 3.5 allows us to calculate the dependence of avalanche energy on avalanche size. The avalanche energy is simply the average squared voltage, $\langle V^2 \rangle$, times the average avalanche duration, $S^{\sigma\nu z}$. Using equation 3.5, this is

$$\begin{aligned} E(S) &= S^{\sigma\nu z} \int_0^\infty V^2 P(V|S) dV \\ &= S^{\sigma\nu z} \int_0^\infty V f(V S^{\sigma\nu z - 1}) dV \\ &\sim S^{2-\sigma\nu z}. \end{aligned} \tag{3.6}$$

Note that this is the same result we would find if we assumed that the time dependence had a square profile.

3.2.4 The scaling of the time-time correlation function with S

With this information, we can calculate the scaling of the time-time correlation function within avalanches, which is simply related to the high-frequency part of the power-spectrum, $\mathcal{P}_{\rm av}(\omega)$. The time-time correlation function is defined as

$$G(\theta) = \int V(t) V(t+\theta) dt. \tag{3.7}$$

If we assume that the magnetic field is increased adiabatically and the avalanches are well separated in time, we can calculate the time-time correlation function separately for each avalanche and then add the individual functions together to get the overall time-time correlation function.[3]

[3]There should also be contributions from cross-terms between avalanches, but this will contribute only at a time θ which grows as the field is ramped more and more slowly. In the limit of

This allows us to break up the time-time correlation function into the contributions from avalanches of different sizes, S. Let $G(\theta|S)$ be the average time-time correlation function of an avalanche, *given* that the avalanche is of size S. (In contrast, the notation $G(\theta, S)$ would denote the contribution of all avalanches of size S to $G(\theta)$. This would be weighted by the probability that an avalanche is of size S, $S^{-\tau}$.) If we consider equation 3.7 at $\theta = 0$, we see that the $\theta = 0$ component of the correlation function is $\int V(t)^2 dt$, which is proportional to the avalanche energy. Using this fact along with the scaling of the energy from equation 3.6, we find that the time-time correlation function should scale as

$$G(\theta|S) = S^{2-\sigma\nu z} f(\theta S^{-\sigma\nu z}). \tag{3.8}$$

As shown in figure 3.4, this scaling works very well over a wide range of avalanche sizes.

3.2.5 The scaling of the energy spectrum with S

The energy spectrum describes the amount of energy released in Barkhausen noise at each frequency. It can be calculated as the cosine transform of the time-time correlation function. Transforming equation 3.8, we find that the scaling of the energy spectrum with avalanche size has the form

$$\begin{aligned} E(\omega|S) &= \int_0^\infty \cos(\omega\theta) G(\theta|S) d\theta \\ &= \int_0^\infty \cos(\omega\theta) S^{2-\sigma\nu z} f(\theta S^{-\sigma\nu z}) d\theta \\ &= S^2 f(\omega^{1/\sigma\nu z} S). \end{aligned} \tag{3.9}$$

an adiabatically slowly increasing field, these cross terms will affect only the $\omega = 0$ scaling of the power spectrum. Here, we are calculating the scaling behavior for large ω.

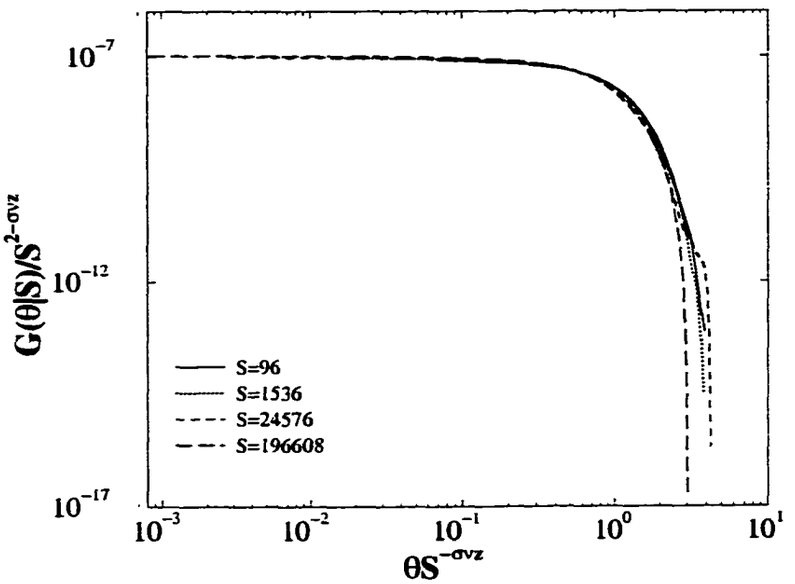

Figure 3.4: A collapse of avalanche time-time correlation functions according to equation 3.8. The data is binned logarithmically to get good statistics.

A collapse of the energy spectra for different avalanche sizes according to this form is shown in figure 3.5.

3.2.6 The energy spectrum scaling depends on the large avalanche cutoff

The energy spectrum for all avalanches (the quantity usually measured in experiments) is just the integral $\int P(S)E(\omega|S)dS$, where $P(S) \sim S^{-\tau}$ is the probability that an avalanche will be of size S. If we substitte equation 3.9 and $P(S) \sim S^{-\tau}$ into the integral, we find the naive prediction

$$\begin{aligned} E_{\text{wrong}}(\omega) &= \int P(S)E(\omega|S) \\ &\sim \omega^{(3-\tau)/\sigma\nu z} \int y^{2-\tau} f_{\text{energy}}(y)dy \\ &\sim \omega^{-(3-\tau)/\sigma\nu z} \end{aligned} \tag{3.10}$$

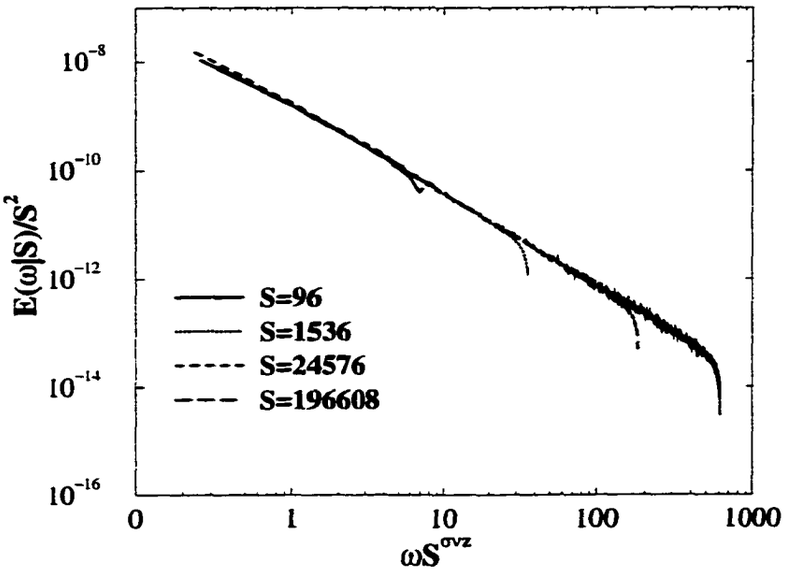

Figure 3.5: A collapse of the energy spectra for different avalanche sizes according to equation 3.9.

as predicted by Lieneweg *et al.*[19], Dahmen and Sethna[3, 6, 11] and Spasojević *et al.*. In the next section we will argue that the energy contributed by an avalanche at fixed frequency ω is proportional to S. This implies that f_{energy} in equation 3.10 should have the form $f_{\text{energy}}(y) \sim A/y$ for large y. The integral in equation 3.10 dies off as a power law $y^{1-\tau}$ for large y. Therefore, the integral gives a well defined (and correct) answer for $\tau > 2$, but for $\tau < 2$ the indefinite integral in equation 3.10 diverges and must be replaced by a definite integral with a cuttoff at large avalanche sizes. The naive result should work for the integrated avalanche size distribution for the short-range model[3, 5] at the critical point R_c. In that case, the corresponding exponent in three dimensions is $\tau + \sigma\beta\delta = 2.03$ (close enough to two that we might expect logarithmic corrections). Above six dimensions, the exponent rises to the mean field value of 9/4. For all of the models which we study in this chapter, $\tau < 2$ and the cutoff at the largest avalanches in hte integral changes the form of the power

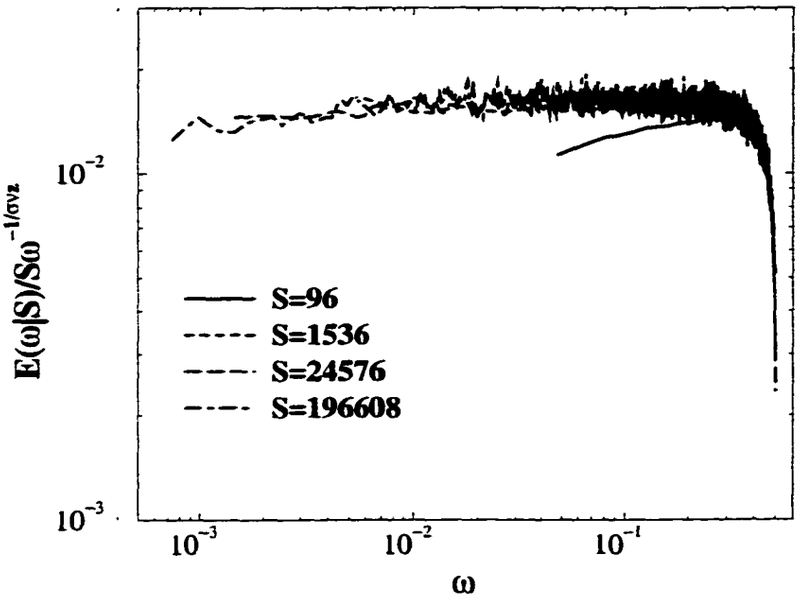

Figure 3.6: A collapse of the energy spectra for several avalanche sizes S. The collapse is performed by dividing out the linear S dependence. The curves are made flat by dividing out the simple power law $\omega^{1/\sigma\nu z}$. The ω axis has not been rescaled, so the high ω cutoffs collapse together and the small ω cutoffs do not.

spectrum.

3.2.7 The energy at frequency ω scale linearly with the avalanche size S?

We shall argue in this section that except at very small frequencies the energy at a fixed frequency is proportional to S. Along with equation 3.9, this eimplies that the energy spectrum at fixed S scales as $\omega^{-1/\sigma\nu z}$. This means that dividing $E(\omega|S)$ by $S\omega^{-1/\sigma\nu z}$ should collapse the curves and eliminate the ω dependence. The resul of this collapse for the infinite range model can be seen in figure 3.6

The fact that the energy at frequency ω scales linearly with S follows from

two assumptions. First, each spin in the avalanche contributes equally to $E(\omega)$. Second, the contribution of a given spin is independent of the size of the avalanche it is in. (Of course, a few spins at the beginning of the avalanche might differ, so long as the fraction of such spins vanishes for large avalanches.) One way in which this could be true would be if the following two hypotheses were true. First, each spin contributes to $E(\omega)$ only through its correlations with physically nearby spins. Second, the local growth of an avalanche does not reflect the overall size of the avalanche. The first hypothesis seems likely in the models described in this paper because the times of physically distant spin flips are likely to be randomly distributed in time and contribute incoherently to the power spectrum. Only nearby spin flips will be correlated in time and contribute coherently. The second hypothesis is also likely to be true because the avalanches are occurring at a critical point. Every part of the avalanche is always on the verge of stopping regardless of the size of the avalanche.

We can check these hypotheses by breaking up the energy spectrum into the contributions from pairs of spins at different radii r. The time-time correlation function for avalanches of size S can be written in terms of individual pairs of spins as

$$G(\theta|S) = \sum_{i,j} \delta(t_j - t_i - \theta), \tag{3.11}$$

where t_i is the time at which spin i flips. From this form, we can use an additional delta function to pull out the contribution due to pairs of spins separated by a distance r:

$$G(\theta, r|S) = \left\langle \sum_j \delta(t_j - t_i - \theta)\delta(|\vec{r}_j - \vec{r}_i| - r) \right\rangle_i , \tag{3.12}$$

where $\langle\rangle_i$ implies an averaging over all values of i. Using this definition of the

function $G(\theta, r|S)$, we can rewrite the time-time correlation function as

$$G(\theta|S) = S \int G(\theta, r|S)dr. \tag{3.13}$$

Now, we can use equation 3.13 to calculate the contribution of spins separated by a distance r to the energy spectrum $E(\omega|S)$ at a frequency ω. Taking the cosine transform of equation 3.13, we find that

$$\begin{aligned} E(\omega|S) &= S \int \int \cos(\omega\theta) G(\theta, r\,|S)drd\theta \\ &\equiv S \int E(\omega, r\,|S)dr, \end{aligned} \tag{3.14}$$

where the function $E(\omega, r\,|S)$ is defined by this equation. Notice that $E(\omega, r\,|S)$ must have a cutoff at the largest r present in an avalanche of size S. We can see from equation 3.14 that in order for $E(\omega|S)$ to be proportional to S, the integral must be independent of this S dependent cutoff. This is a more precise statement of the hypothesis that only correlations between nearby spins contribute to the energy spectrum. It is also necessary that except for extreme values of ω and r, $E(\omega, r\,|S)$ must be independent of S. Combined with the first condition, this corresponds to the hypothesis that the local growth of the avalanche should not reflect the overall size of the avalanche.

Figure 3.7 shows that the decay of $E(\omega, r\,|S)$ is decaying approximately as $1/r$. Figure 3.8 shows that it is independent of S and that the decay is oscillating about zero. Neighboring radial shells contribute with opposite sign. Hence the integral 3.14 appears to be conditionally convergent at large distances: each spin contributes to $E(\omega)$ only through its correlations with nearby spins, and $E(\omega|S) \sim S$.

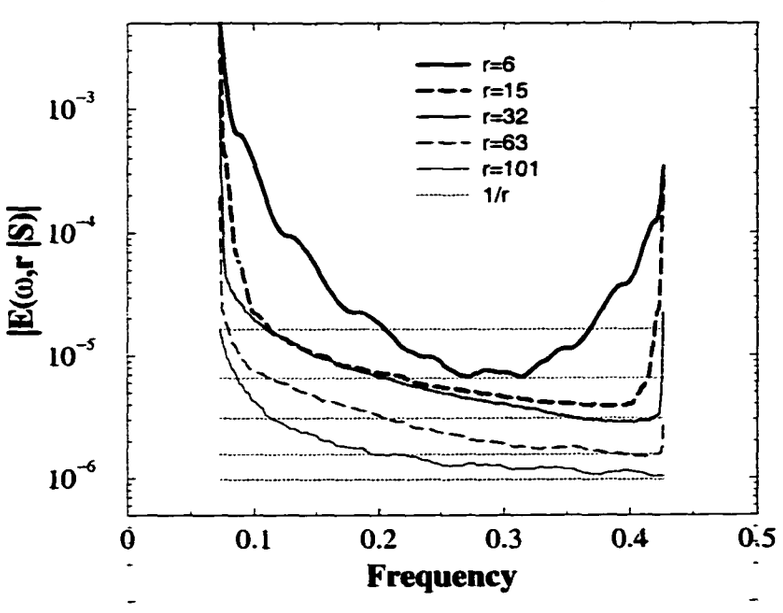

Figure 3.7: This graph shows the function $|E(\omega, r\,|S)|$ for a range of values of r at $S = 32500$. The function $E(\omega, r\,|S)$ not only decays with ω, but also oscillates about zero. To better compare the amplitudes of the curves at different r, we took the absolute value and performed a running average over ω, averaging out the oscillations. The horizontal lines show how the positions of these curves should scale if they went as $1/r$. Notice that while for small r the amplitudes drop slower than $1/r$, for larger r the amplitudes drop off approximately as $1/r$.

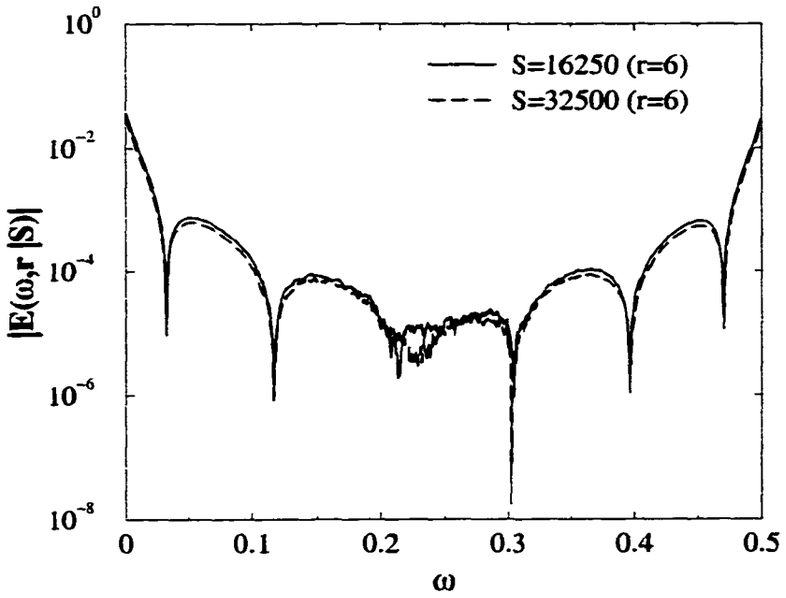

Figure 3.8: This graph shows $|E(\omega, r\,|S)|$ at $r = 6$ for two sizes of avalanches. No averaging has been performed, so the oscillations are visible (the function changes sign at each dip). For larger r, the oscillations are much faster. Notice that the curves are nearly identical for the two sizes—$E(\omega, r\,|S)$ has no significant S dependence at small r.

3.2.8 Integrating the energy spectrum over avalanche sizes

In section 3.2.6 we found that in order to understand the scaling of the energy spectrum for $\tau < 2$, we must first understand the cutoff at large avalanche sizes. In our simulations, there is a typical largest avalanche size S^* which is primarily due to finite size effects: $S^* \sim L^{1/\sigma\nu}$. In experiments, the typical largest avalanche size could be determined by the finite experimental duration or from the demagnetizing forces. (In some cases, demagnetizing forces also contribute to the cutoff in our simulations.) These effects would cut off the probability of getting large avalanches.

For large avalanches, the contribution to $E(\omega)$ from an avalanche of size S scales linearly in S: each spin contributes the same amount. The cutoff at large avalanche sizes dominates the scaling of $E(\omega)$ precisely because most spins are in the largest avalanches. The distribution of avalanche sizes $D(S, S^*)$ cannot be a simple power law cut off at S^* for $\tau < 2$, because we know that $\int SD(S, S^*)dS = 1$, but $\int^{S^*} S^{1-\tau}dS$ depends on S^* and diverges as $S^* \to \infty$. Hence, the overall amplitude of D must decrease as S^* gets bigger. If we describe the avalanche size distribution with an amplitude depending on S^*, we can solve this problem:

$$D(S, S^*)dS = (S^*)^{-2} f_{\text{size}}(S/S^*) \tag{3.15}$$

$$f_{\text{size}}(y) \sim y^{-\tau} \quad y \to 0 \tag{3.16}$$

$$\begin{aligned} \int SD(S, S^*)dS &= \int (S^*)^{-2} S f_{\text{size}}(S/S^*)dS \\ &= \int y f_{\text{size}}(y)dy \\ &= 1 \end{aligned} \tag{3.17}$$

where the last equation provides a condition on the scaling function f_{size}.

We are now ready to integrate the power spectrum over S, finding the form $E(\omega)$ corresponding to equation 3.10, but valid for $\tau < 2$. We found in the last section

that $f_{\text{energy}} \to A/y$. We control the integral by adding and subtracting A/y:

$$\begin{aligned} E(\omega) &= \int D(S,S^*)E(\omega|S)dS \\ &= \int [(S^*)^{-2} f_{\text{size}}(S/S^*)][S^2 f_{\text{energy}}(\omega^{1/\sigma\nu z}S)]dS \\ &= \int (S/S^*)^2 f_{\text{size}}(S/S^*) f_{\text{energy}}(\omega^{1/\sigma\nu z}S)dS \\ &= \int (S/S^*)^2 f_{\text{size}}(S/S^*) A/(\omega^{1/\sigma\nu z}S)dS \\ &+ \int (S/S^*)^2 f_{\text{size}}(S/S^*)[f_{\text{energy}}(\omega^{1/\sigma\nu z}S) - A/(\omega^{1/\sigma\nu z}S)]dS \end{aligned} \tag{3.18}$$

In the first integral, we set $z = S/S^*$. In the scond integral, we set $y = \omega^{1/\sigma\nu z}S$. Also, the second integral now converges, so we can substitute $f_{\text{size}}(S/S^*) \to (S/S^*)^{-\tau}$:

$$\begin{aligned} E(\omega) &= \omega^{-1/\sigma\nu z} \int Az^2 f_{\text{size}}(z)dz \\ &+ (S^*)^{\tau-2}\omega^{-(3-\tau)/\sigma\nu z} \int y^{2-\tau}[f_{\text{energy}}(y) - A/y]dy \end{aligned} \tag{3.19}$$

$$\sim \omega^{-1/\sigma\nu z} \qquad (\tau < 2) \tag{3.20}$$

The exponent in the second term of equation 3.19 is E_{wrong} of equation 3.10, given by ignoring the cutoff at large avalanche sizes. However, for $\tau < 2$ the first term will dominate over the second term both for large system sizes and for large ω. Only for $\tau > 2$ will the second term dominate. For all of the models we are considering in this chapter, $\tau < 2$. (See table 3.1.) In fact, the exponent $(3-\tau)/\sigma\nu z$ disagrees badly with the results obsered in both simulation and experiments, and the exponent $1/\sigma\nu z$ agrees very well. In mean field theory, we can actually derive rigorously that the power spectrum exponent is 2 (see appendix A). This is in perfect agreement with the exponent $1/\sigma\nu z$ and in complete disagreement with the exponent $(3-\tau)/\sigma\nu z$ which would be 3. A plot of the power law for the infinite-range model can be seen in figure 3.9. A comparison of the two possible exponents with simulations for each of the three models can be seen in table 3.2.

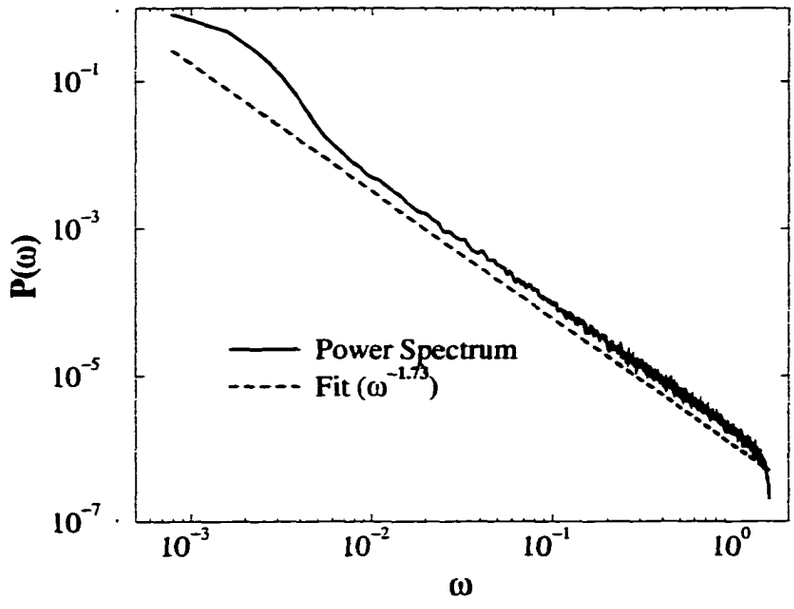

Figure 3.9: The power spectrum for the infinite range model. The dashed line is not a fit. It is a power law with an exponent $1/\sigma\nu z$.

Table 3.2: This table compares values of the power spectrum exponent measured in simulations with the values predicted by the exponents $1/\sigma\nu z$ and $(3-\tau)/\sigma\nu z$. Notice that for all three models $1/\sigma\nu z$ is very close to the simulated exponent, and $(3-\tau)/\sigma\nu z$ is in complete disagreement.

	$1/\sigma\nu z$	$(3-\tau)/\sigma\nu z$	Simulated
Short-range	1.72	2.41	1.70
Infinite-range	1.72	3.00	1.70
Dipole	2.00	3.00	2.00

3.3 How universal is the exponent $1/\sigma\nu z$?

We have shown quite generally that the non-universal scaling of the high ω cutoff in $E(\omega|S)$ causes the naive exponent of $(3-\tau)/\sigma\nu z$ to be incorrect whenever $\omega^{(3-\tau)/\sigma\nu z}$ decays more rapidly than $E(\omega|S)$. (In our models, where we have shown that $E(\omega|S) \sim \omega^{-1/\sigma\nu z}$, this occurs for all $\tau < 2$.) Instead, the exponent of the overall energy spectrum $E(\omega)$ is the same as the exponent for the energy spectrum for avalanches of a fixed size S, $E(\omega|S)$. However, the conclusion that the exponent for the energy spectrum at fixed S was $1/\sigma\nu z$ was based on less general arguments. In fact, for models with very different dynamics, it is likely that the exponent will not be $1/\sigma\nu z$.

So far, we have only verified these results for the infinite range model in three dimensions. However, we have also checked these results in several other situations where both τ and $\sigma\nu z$ take on a range of values. (In all cases, $\tau < 2$.) We have checked the short-range model in 3 and 4 dimensions, the infinite-range model in 3 and 4 dimensions, and mean field theory. In all cases, the linear scaling with S seems exact, and both $E(\omega|S)$ and $E(\omega)$ scale as $\omega^{-1/\sigma\nu z}$ to within simulational precision. In all cases, the exponent $(3-\tau)/\sigma\nu z$ is completely inconsistent with the observed results. The results of mean field theory and the short-range model at the three dimensional critical point can be seen in figures 3.10 and 3.11. The results for the four dimensional short-range model and the four dimensional infinite range model were also completely consistent with a $1/\sigma\nu z$ scaling exponent.

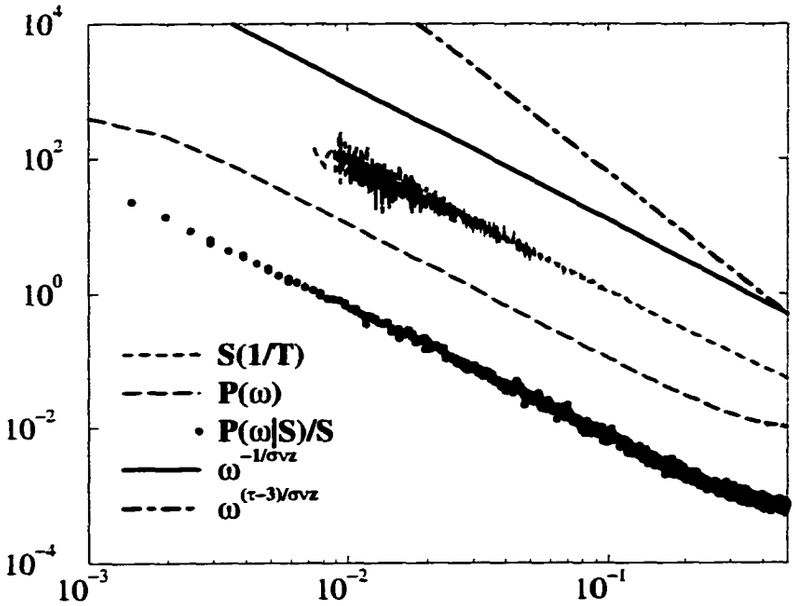

Figure 3.10: The mean field model. Notice that the energy spectrum for avalanches of size S collapses when divided by S, and that the energy spectrum for avalanches of size S and the overall energy spectrum both have the same power law as the average avalanche size as a function of the inverse avalanche duration. Sizes 96, 1536, 24576, and 196608 are shown in the collapse of $P(\omega|S)/S$. The average avalanche size as a function of the inverse avalanche duration is the definition of the exponent $1/\sigma\nu z$. Power laws of $1/\sigma\nu z$ and $(3-\tau)/\sigma\nu z$ are also shown for comparison. Notice that $(3-\tau)/\sigma\nu z$ is completely incompatible with the results.

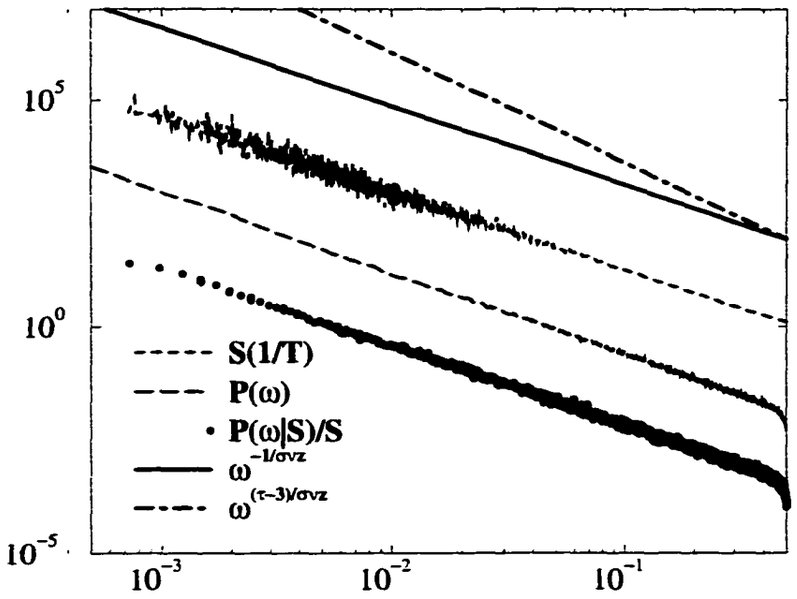

Figure 3.11: The short-range model in 3 dimensions. The plots and the sizes are the same as in figure 3.10.

3.4 Discussion

There have been several previous predictions of the power spectrum exponent. In her Ph.D. thesis, Karin Dahmen[11] did a calculation similar to the one done in this paper, but she ignored the problems with the integral and came up with the exponent $(3-\tau)/\sigma\nu z$. This exponent was published by our group[3] without any derivation, and was compared to experimental work by Cote and Meisel[20, 21] and Bertotti *et al.*[22] The correct exponent form derived here makes the agreement between the short-range model and these experiments substantially better: they quote an exponent of "around 2", our former (wrong) prediction was 2.46 ± 0.17, and the correct prediction is 1.75 ± 0.25. Spasojević, Bukvić, Milosević and Stanley[8] also came up with the same (wrong) form based on arguments about the average pulse shape. They measured an experimental power spectrum exponent of 1.6. For their experimentally determined values of $\tau = 1.77$ and $\sigma\nu z = 0.662$, they found

that $(3-\tau)/\sigma\nu z = 1.86$ fit their data well, but the value of $(3-\tau)/\sigma\nu z = 2.46$ quoted by Dahmen et. al.[3] was much too large. This lead them them to disregard the plain old critical model with domain nucleation as a possible explanation of Barkhausen noise in their system. However, note that their experimental value of $1/\sigma\nu z = 1.51$ is as close to their measured power spectrum exponent as their value of $(3-\tau)/\sigma\nu z = 1.86$. The value of $1/\sigma\nu z = 1.75 \pm 0.25$ quoted by Dahmen *et al.* is even closer to the experimentally observed power spectrum exponent. The value of $\tau = 1.6$ predicted by Dahmen *et al.* is also closer to the experimentally measured $\tau = 1.77$ than any of the other models. (Front propagation has an exponent $\tau = 1.3$, and mean-field theory has an exponent $\tau = 1.5$.) One should note, however, that the average avalanche shapes measured by Spasojević *et al.* disagree with those predicted by the short-range model (figure 3.2).

In 1989, Jensen, Christensen and Fogedby[13] published a different calculation of the power spectrum exponent for sandpile models, which has been cited many times as an explanation for $1/\omega^2$ scaling of the power spectrum in sandpiles, Barkhausen noise, and other systems. They made two major assumptions in their derivation. First, they assumed that the avalanche shape could be approximated by a box function: $V(t) = S/T$ for all $t < T$. For our models, this assumption turns out to be valid for calculating the average avalanche energy, but is not valid for determining the overall scaling of the time-time correlation function. Second, they assumed that one of their scaling functions, which was related to the time-time correlation function, had the simple scaling form $G(T) \sim T^{\alpha}\exp(-T/T_0)$. As can be seen from the exact mean field time-time correlation function in equation A.6, this is not at all a safe assumption. In terms of our exponents τ and $\sigma\nu z$, their prediction was that the energy spectrum would have the form $E(\omega) \sim \omega^{(3-\tau)/\sigma\nu z}$ for $\tau > 3 - 2\sigma\nu z$

and $E(\omega) \sim \omega^{-2}$ for $\tau < 3 - 2\sigma\nu z$. This is the same as our result in the case where $\sigma\nu z = 1/2$. For the particular model they were studying, their assumptions seem to be correct, but in the more general case, the exponent $(3-\tau)/\sigma\nu z$ should become invalid for $\tau < 2$, rather than $\tau < 3 - \sigma\nu z$. Also, for $\tau < 2$, exponents other than 2 are possible, depending on the particular dynamics. For the class of models described in this paper, the correct exponent for $\tau < 2$ is $1/\sigma\nu z$.

There are other specific models for which the power spectrum exponent has been calculated. For example, Bak, Tang and Wiesenfeld[23] calculated the power spectrum exponent for their sandpile models. Without further investigation, we can't expect our arguments for an exponent of $1/\sigma\nu z$ to hold for these and other models. However we do expect that in any avalanche based model, the power spectrum exponent for $\tau > 2$ will be $(3-\tau)/\sigma\nu z$, and another exponent will dominate for $\tau < 2$. Whenever the arguments in section 3.2.7 hold, we expect that for $\tau < 2$ the exponent $1/\sigma\nu z$ will dominate. (Where $1/\sigma\nu z$ is the exponent relating avalanche size to avalanche duration.)

Chapter 4

Scaling in two dimensions

Previous work by Jim Sethna, Karin Dahmen, Olga Perkovic and others has thoroughly described the behavior of the zero-temperature random-field Ising model in three dimensions and higher. However, the behavior in two dimensions is still poorly understood. For small systems (and for the large disorders which are necessary in small systems) the scaling seems quite good with the same scaling forms used in three dimensions and higher. However, as larger and larger systems are run, at lower and lower disorders, the scaling seems to break down. Using large simulations at small disorder, we argue here that R_c is zero, and that the scaling variable takes on an unusual form $r^2 \log s$.

4.1 Scaling the avalanche size distribution in 2D

One of the most important scaling functions in three and higher dimensions is the avalanche size distribution (integrated over H), $P(S)$. The standard scaling form for the avalanche size distribution is

$$P(S) = S^{-\tau+\sigma\beta\delta} D(rS^{\sigma}), \tag{4.1}$$

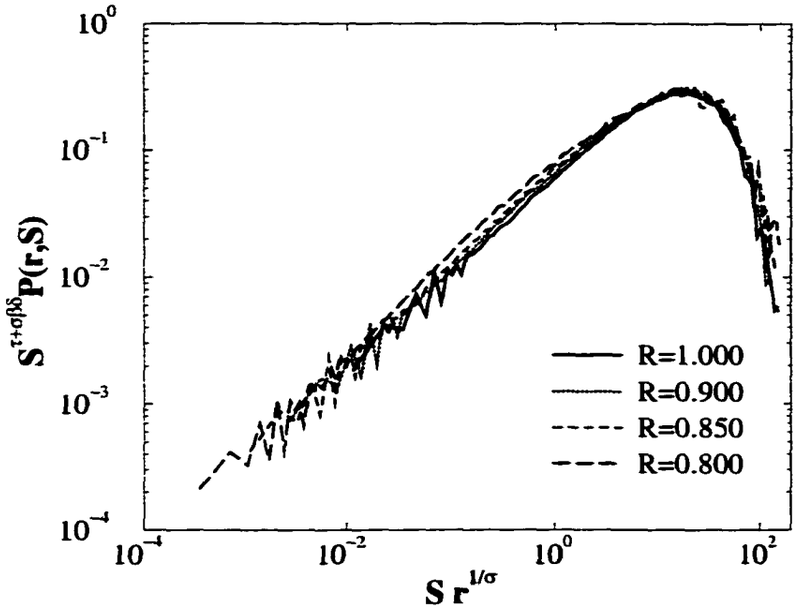

Figure 4.1: Large disorders collapse well.

where τ is the distance from the critical disorder, $\frac{R-R_c}{R_c}$, S is the avalanche size, and $\tau + \sigma\beta\delta$ and σ are relevant scaling exponents. For large disorders, this scaling form seems to work quite well. Figure 4.1 shows the scaling for high disorders with $R_c = 0.63$, $\tau + \sigma\beta\delta = 2.04$ and $1/\sigma = 4.5$. Notice that while the scaling is quite good, and all of the peaks collapse together, the lowest disorder curve ($R = 0.8$) seems to have a slightly different shape from the other curves. There is a bump at smaller avalanche sizes which cannot be collapsed. If this $R = 0.8$ curve had been dropped, as would be necessary if we were running systems only a few hundred spins on a side, it would seem quite reasonable to concluding that there was a standard scaling form, with $R_c = 0.63$ and $1/\sigma = 4.5$.

However, as can be seen in figure 4.2, the situation becomes much worse when larger systems are used and smaller disorders are studied. The bump rapidly grows until only the peaks (and eventually not even the peaks) collapse well. Because the shape and the slopes are changing as the disorder is lowered, no scaling form which

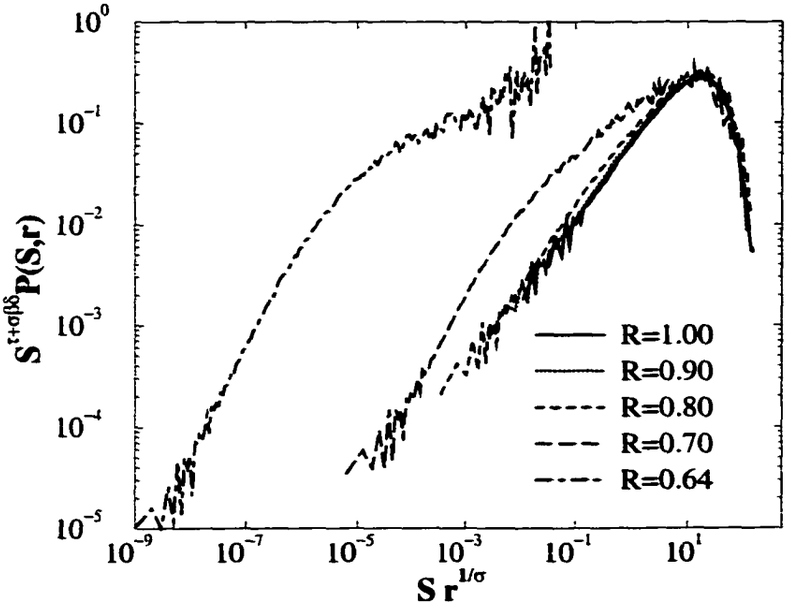

Figure 4.2: No horizontal translations can fix this bump at lower disorders!

simply translates the curves horizontally (like the standard scaling form in higher dimensions) could possibly fix this problem. Moreover, with a 30000×30000 system, there are still no system spanning avalanches for disorders *below* $R = 0.63$.

A hint to a potential solution of this problem comes from the fact that $1/\sigma = 4.5$ seems quite large. (Though it was already almost as large, $1/\sigma = 4.2$ in three dimensions) If two was the lower critical dimensions of the system, then it would be typical for the critical exponents to be ratios of small integers. What if in reality $\sigma = 0$? In this case, the standard scaling form would not be meaningful.

In her Ph.D. thesis, Olga Perković performed a very elegant derivation of two possible scaling forms for the case $\sigma = 0$. The first scaling form assumed $R_c \to 0$ in two dimensions, and the second scaling form didn't. If $R_c = 0$, she concluded that the scaling variable would be $s\exp(1/(lr^2))$ instead of $sr^{1/\sigma}$. If $R_c > 0$, she concluded that the scaling variable would be $s\exp(1/(kr))$. These scaling forms were also suggested by Bray and Moore in the context of the thermal RFIM. ([24])

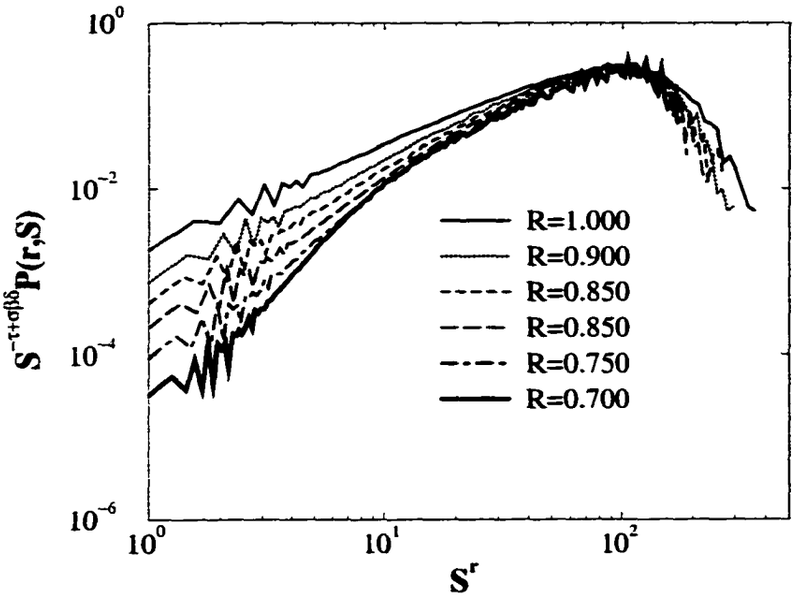

Figure 4.3: The scaling variable s^r gives a good collapse.

Unfortunately, these scaling variables both merely translate the avalanche size distribution horizontally without any possibility of correcting the slope change associated with the bump.

The naive guess for a $\sigma = 0$ equivalent of $s^\sigma r$ is $r \log(s)$. This is actually the $\sigma \to 0$ limit of $(s^\sigma - 1)r/\sigma$. This is analogous to the logs that appear at the upper critical dimension. It turns out that this scaling form, though seemingly on weaker theoretical grounds than the scaling forms Olga derived, works very well at much lower values of R. Notice that unlike the other three scaling forms, it *does* change the shape of the curve. Figure 4.3 shows a collapse using an equivalent scaling variable r^s. The critical disorder $R_c = 0.39$ derived from this collapse is *much* lower than the value of $R_c = 0.63$ derived from the incorrect scaling form at large R. Not only do the peaks collapse well, but down to about $R = 0.7$, the bump in the scaling form collapses well with this scaling form.

Unfortunately, as we increase the system size even farther, to 46000^2, and push

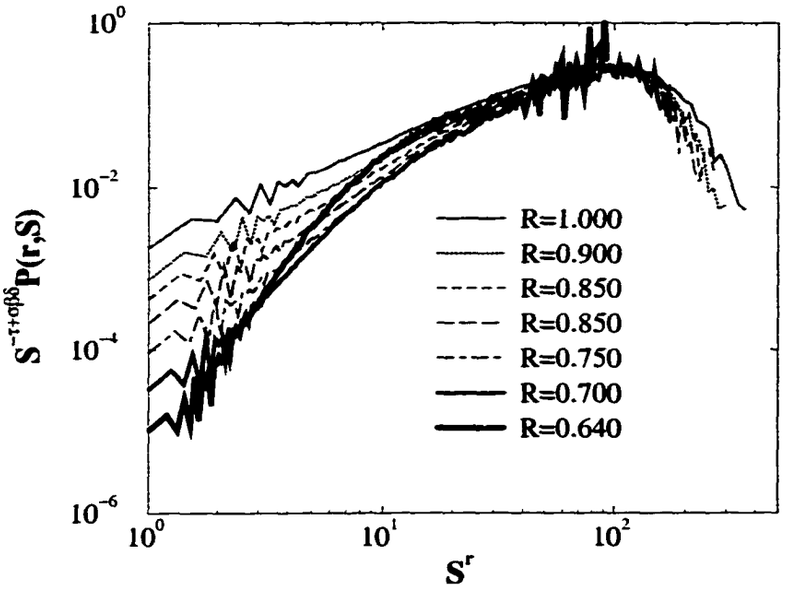

Figure 4.4: At low enough disorders (requiring $45,000 \times 45,000$ simulations!) the scaling becomes bad again.

the disorders down to $R = 0.64$, the scaling breaks down once again, and this form, too, does not work. This breakdown in scaling is shown in figure 4.4. Moreover, although this scaling seems to indicate that we are well above R_c, the hysteresis loop goes from almost smooth (for a two billion spin system) at $R = 0.64$ to having an enormous jump at $R = 0.6$. The two hysteresis loops are shown in figure 4.5. The largest avalanche at $R = 0.64$ was about 100,000,000 spins. The largest avalanche at $R = 0.60$ was about 1,800,000,000 spins (18 times larger), and would have been larger in the absence of finite size effects! This indicates a much larger change in correlation length than would be expected if the scaling shown in figure 4.3 were correct.

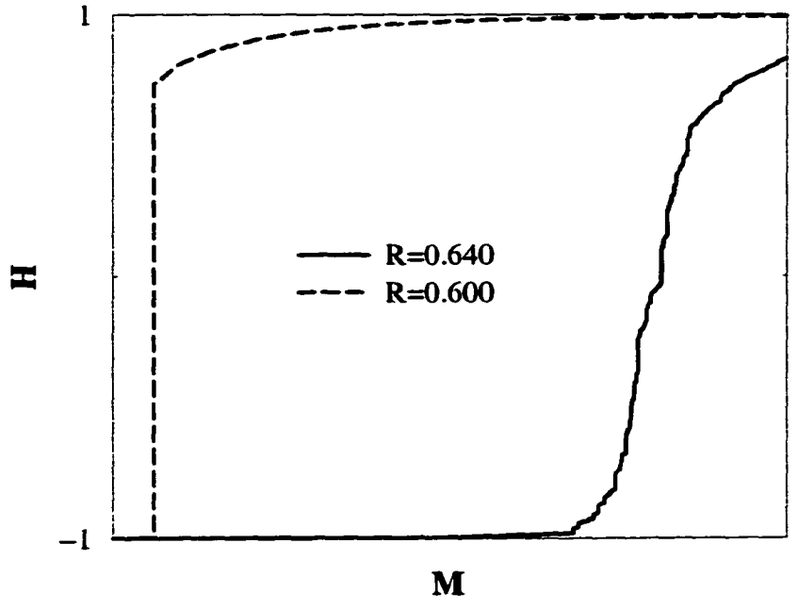

Figure 4.5: Between $R = 0.64$ and $R = 0.60$, the correlation length increases drastically, and the hysteresis loops goes from a smooth one to one with most of the system flipped in a single avalanche. This is inconsistent with a critical disorder of $R = 0.38$. It is much more consistent with the critical disorder predicted by the standard scaling form, but this form does not successfully collapse the data near R_c.

4.2 Is there a problem with nucleation?

Even for very large systems, there appears to be a problem with nucleation in two dimensions. In the thermodynamic limit, even for very low disorders, there would be a few spins, or even clusters of spins, which would flip long before other spins. However, for the system sizes we can study in simulations, even for two billion spins, there are very few spins available to nucleate the initial avalanche. This difficulty in nucleation might lead to distorted distributions of avalanches.

Hoping that this was the source of our problems with scaling in two dimensions, we tried to alleviate the nucleation problem in several ways. The first thing we tried was to add a row of preflipped spins to the simulation, so that the initial avalanche nucleation would be easier. This lead to growth very similar to the front propagation described by Robbins *et. al.* [7], with only a few clusters of flipped spins in front of the advancing front. Though this qualitatively changed the early portion of the magnetization process, it did not change the avalanche size distributions, and our scaling problems remained.

We also tried using a random field distribution with much longer tails, so that there would be more spins capable of flipping early. The distribution we chose was a Lorenzian distribution:

$$\rho(h) = \frac{1}{a\pi}\frac{1}{a^2 + h^2}. \tag{4.2}$$

Indeed, with this distribution many spins flipped alone or in small clusters early in the simulation, providing many potential sites for avalanche nucleation. However, this only changed the small S, non-universal part of the avalanche size distribution, leaving the scaling unchanged.

4.3 Are there symmetry problems?

Another possibility we considered was the possibility that there was some sort of asymmetry (perhaps between the horizontal/vertical directions and the diagonal directions) which only became important when the correlation length became very large. We did two things to test this. First, we compared horizontal correlation functions with diagonal correlation functions. We found that these correlation functions differed only at distances of a few lattice spacings.

Second, we tried using different lattices with different symmetries. We tried running simulations on both triangular and hexagonal lattices. The only effect of this change was to change the value of the apparent critical disorder. The critical behavior was completely unchanged. In fact, with a shift of coordinates to account for changing values of R_c, the square lattice results, the triangular lattice results, the hexagonal lattice results, and the Lorenzian square lattice results could all be collapsed on top of each other. (*Including* the growth of the bump.)

4.4 Is there a problem with the random number generator?

We also worried that with the very large simulations we were running, we might be running into problems with correlations in the random number generator. To examine this problem, we tried using several different high quality random number generators. We found that the different random number generators produced statistically identical simulational results. We also tried using two different algorithms for medium sized simulations (large enough to begin seeing the growth of the bump)—the sorted list algorithm and the bits algorithm, as described in chapter 5. Even

though these algorithms use random numbers in completely different ways, we got statistically identical results.

4.5 Good scaling at last

In the final days before the oral defense of this Ph.D, we tried yet another scaling variable, $r^2 \log s$ (or, equivalently, s^{r^2}), with $R_c = 0$. This was motivated by three things.

1. Figure 4.5 suggested that the largest avalanches grow very quickly with decreasing disorder; for this scaling form, the largest avalanches grow as $\log s \sim \frac{1}{r^2}$. This is faster than any of the previous forms.

2. In the thermal RFIM [24], the correlation length was conjectured to grow as le^{A/r^2}, which implies that the largest avalanches grow as $\log s \sim \frac{1}{r^2}$. Perhaps they got the scaling variable wrong, but got the relationship between the largest avalanches correct.

3. This form is natural for $R_c = 0$; since $R \rightarrow -R$ is a symmetry of the model, odd powers of R are not expected. Since $R_c = 0$ in the two dimensional thermal RFIM, and $R_c = 0$ has been argued for the front propagation version of our model[25], it seems reasonable to expect $R_c = 0$ in our model. Finally, since no spins can flip ahead of the infinite avalanche at $R = 0$, our model becomes equivalent to the front propagation model if $R_c = 0$.

As one sees from figure 4.6, this scaling form works quite well.

We note three key points in brief:

1. It would seem likely that the correct scaling variable for the thermal RFIM

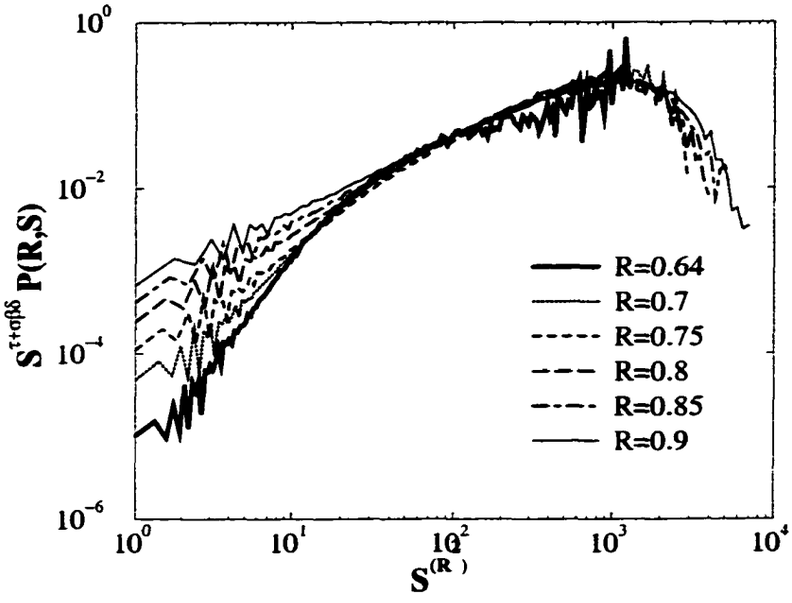

Figure 4.6: The scaling variable appears to be $r^2 \log s$, or equivalently s^{r^2}; R_c appears to be zero.

may also be $r^2 \log s$. This may not be testable in the near future, as simulations of this model are currently confined to *much* smaller systems. We saw in the zero temperature model that very large systems were necessary to rule out traditional scaling forms.

2. There are many cases where logarithms of physical quantities are the scaling variables. Two that come to mind are the metal-insulator Anderson transition in one dimension [26] (where the scaling variable involves $\log(1+\rho)$ with ρ the dimensionless resistance) and the random transverse field Ising chain (where $\log \frac{\Delta E}{L^{1/2}}$ is a scaling variable with ΔE the energy gap)[27, 28, 29].

3. Having the logarithm of a physical *size* be the scaling variable strikes at the heart of the renormalization group as it is usually formulated! Since the renormalization group coarse-graining is done in space, lengths and areas are treated

differently than conductivities and energy distributions. It would appear that an unorthodox approach will be necessary in two dimensions.

Chapter 5

Algorithms for simulating the zero temperature RFIM

In our studies of hysteresis and avalanches in a simple model of magnetism (the random-field Ising model at zero temperature), we have often found it necessary to do very large simulations. Previous simulations were limited to relatively small systems (up to 900^2 and 128^3 [30, 31], with the exception of Ji and Robbins[1]). In our simulations we have found that larger systems (up to a billion spins) are crucial to extracting accurate values of the universal critical exponents and understanding important qualitative features of the physics. As we need larger and larger simulations, the scaling of time and memory become more and more important.

We have developed two efficient and relatively straightforward algorithms which allow us to study large systems for the short-range model. The first algorithm uses sorted lists and scales as $O(N \log N)$, and asymptotically uses

[1] Ji and Robbins [7] study the closely related interface depinning model (which does not allow avalanches to start except next to existing flipped spins). The methods we discuss in this chapter can be used to study front propagation (by pre-flipping a layer of spins and setting the probability of flipping isolated spins to zero), but are less efficient than those developed by Ji and Robbins, which "forget" the spins left behind by the propagating interface. They ran 300^3 and 2000^2 simulations in 1991 and 12000^2 simulations in 1994.

$N \times$ (sizeof(double)+sizeof(int)) bytes of memory, where N is the number of spins. This algorithm can also be extended to support infinite range forces. The second algorithm, which does not generate the random fields, also scales in time as $O(N \log N)$, but asymptotically needs only one bit of storage per spin, about 96 times less than the first algorithm. Neither algorithm can be used when dipole-dipole interactions are present. Using the latter algorithm, simulations of a billion spins can be run on a workstation with 128MB of RAM in a few hours.

The algorithms discussed in this chapter can be used to simulate the following simplified version of the Hamiltonian in equation 2.2:

$$\mathcal{H} = -\sum_{<i,j>} J s_i s_j - \sum_i [H(t) + h_i] s_i, \tag{5.1}$$

where the spins $s_i = \pm 1$ sit on a D-dimensional hypercubic lattice[2] with periodic boundary conditions. The spins interact ferromagnetically with their z nearest neighbors with strength J, and experience a uniform external field $H(t)$ and a random local field h_i. We choose units such that $J = 1$. The random field h_i is distributed according to the Gaussian distribution[3] $\rho(h)$ of width R:

$$\rho(h) = \frac{1}{\sqrt{2\pi}R} e^{-h^2/2R^2}. \tag{5.2}$$

The external field $H(t)$ is increased arbitrarily slowly from $-\infty$ to ∞.

The dynamics of our model includes no thermal fluctuations: each spin flips deterministically when it can gain energy by doing so. That is, it flips when its local field

$$h_i^{\text{eff}} = J \sum_j s_j + h_i + H \tag{5.3}$$

[2]We have also examined this model on triangular and hexagonal lattices, and found the same critical behavior. The models discussed here can be applied relatively easily to these other lattices.

[3]Other distributions are also possible. For a wide range of distributions, the critical behavior will be the same. We have applied the algorithms in this paper to both Gaussian and Lorenzian distributions.

changes sign. This change can occur in two ways: a spin can be triggered when one of its neighbors flips (by participating in an avalanche), or a spin can be triggered because of an increase in the external field $H(t)$ (starting a new avalanche).

The zero-temperature random-field Ising model is interesting because, as in the disordered magnetic materials it attempts to model, the avalanches can have a broad range of sizes. If all the avalanches were small, understanding them would be straightforward and not very interesting. Indeed, at large disorder R, the chance that a spin which has just flipped will trigger one of its z neighbors scales roughly as zJ/R. If this quantity is smaller than one (large disorder), all avalanches will be small: the noise will be a series of small pops all of about the same size. This behavior is uninteresting not because it is simple, but because the behavior is strongly dependent on the details of the model at short distances, where the model is at best a caricature of a real material.

It also is easy to understand the system in the small disorder regime $zJ/R >> 1$, where almost all the spins flip over in one infinite avalanche. There are many problems (for example, fracture and first-order phase transitions) where a single nucleation event leads to the release of the stored energy in a single catastrophic event.

We focus on the crossover between these two limiting cases, where the system exhibits crackling noise with avalanches of all sizes. For a particular value of the disorder $R = R_c$, a spin which has just flipped will on average flip exactly one neighbor as the external field $H(t)$ is increased to a particular value H_c. The avalanches at R_c, H_c (the critical point), are finely balanced between halting and growing forever. They advance in fits and starts (see Figs. 5.1 and 5.2) and come in all sizes (Figs. 5.3 and 5.4) with a probability which decreases as a power law of the number of spins in

the avalanche. At H_c, the distribution of avalanche sizes decays with an exponent of $\tau \approx 1.6$ (quite close to the experimental results), and integrated over all H, the distribution decays with an exponent[4] $\tilde{\tau} \approx 2$. Below the critical disorder R_c, there will be an avalanche which will flip a nonzero fraction of the spins in the system even as the system size goes to infinity: we call this the infinite avalanche. There are very large avalanches even for disorders far above the critical disorder. In three dimensions, there are still two decades of power law scaling 50% above the critical point. However, the convergence to the expected asymptotic power law is very slow. (Figure 5.3) This behavior means that we see critical scaling even if we do not fine tune R to R_c, but we must use very large systems to get close enough to R_c to get a convincing power law. In practice, we needed simulations of approximately a billion spins to understand the physics in three dimensions [4]. As described in chapter 4.1, the proper scaling in two dimensions remains unclear even for systems of size $46,000^2$.

It is crucial in simulations with this many spins that our algorithms be efficient both in computer time and memory. We begin by giving the simple, but inefficient approach which has an execution time which scales as $O(N^2)$. We then develop a more efficient approach using a sorted list which gives an execution time that scales as $O(N \log N)$, but which needs memory storage which scales as $N \times$ (sizeof(double)+sizeof(int)). A billion spins would demand 12 Gigabytes of RAM for efficient execution, which usually is not available. Finally, we give an algorithm whose execution time also scales as $O(N \log N)$, but whose memory requirements asymptotically are only one bit per spin. In this case 10^9 spins requires 120 MB of storage, which is feasible on a standard workstation [5]. We conclude with

[4]The exponent $\tilde{\tau}$ can be written in terms of other critical exponents for our problem: $\tilde{\tau} = \tau + \sigma\beta\delta$.

[5]Neither of the useful algorithms parallelizes well; our group has made effective and extensive

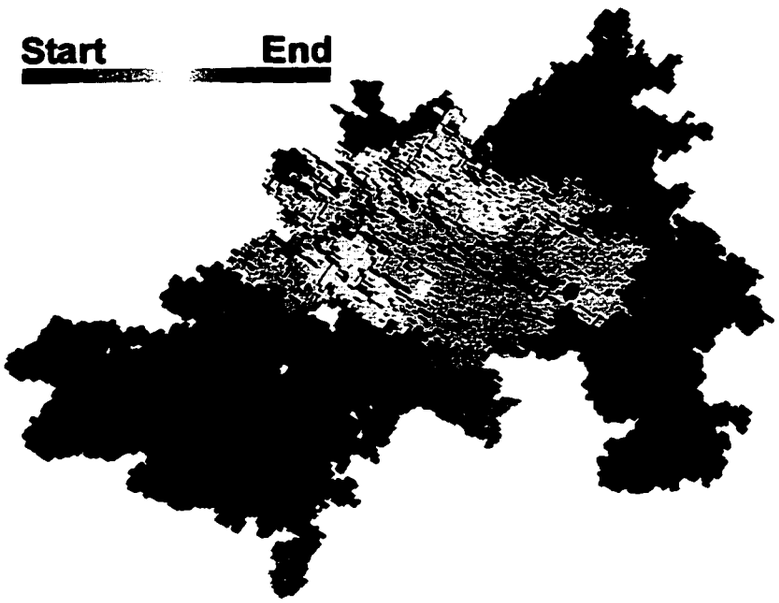

Figure 5.1: A three dimensional view from one side of a single avalanche in a $200 \times 200 \times 200$ system at $R = 2.3$ (within 6% of the critical disorder R_c). The avalanche contains 282,785 spins. The time when each spin flipped is shown by its color. The avalanche generally grew from left to right. Notice that it has many branches and holes; the large avalanches in three dimensions probably have a fractal dimension a little less than three. Also notice that on the right hand side, in the middle of the light green area, there are several dark red spots poking through. The green area stopped growing, but other parts of the avalanche later filled in the holes.

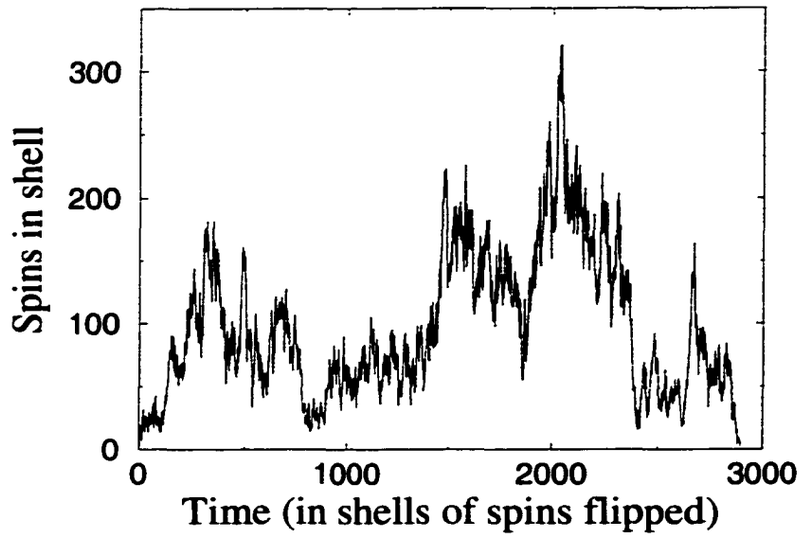

Figure 5.2: A time series showing the number of spins that flipped in each shell of the avalanche shown in Fig. 5.1 [32]. Note that the avalanche is a series of bursts: near the critical point, the avalanche is always on the verge of halting, so it proceeds in fits and starts.

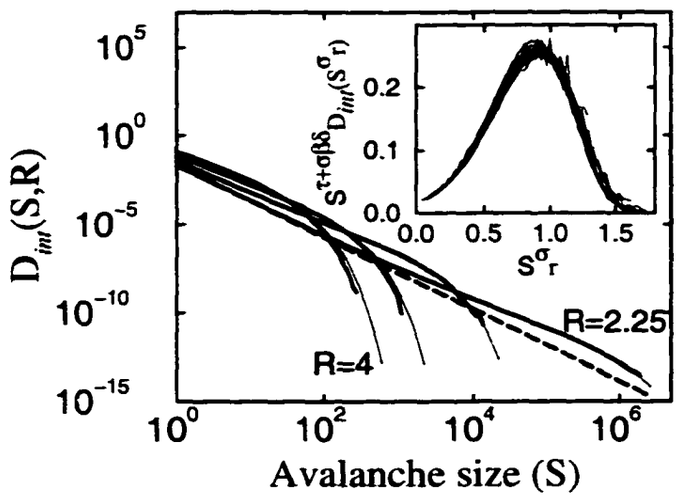

Figure 5.3: Distribution of avalanche sizes for different values of the disorder R in three dimensions. Some avalanches remain large (hundreds of spins) for R a factor of two above the critical value $R_c \sim 2.16$ where we expect a pure power law. The avalanches are enormous (millions of spins) when the system is still 4% away from the critical point; for this reason we need large systems. The inset is a scaling collapse of the data: the thin lines in the main figure show the scaling prediction for the avalanche sizes stemming from the scaling collapse[4]. Notice that the scaling predictions already work well at $R = 4$. The pure asymptotic power law behavior is not yet seen at $R = 2.25$, when six decades of scaling are observed. We needed simulations of a billion spins to show convincingly that the power law would eventually occur[4].

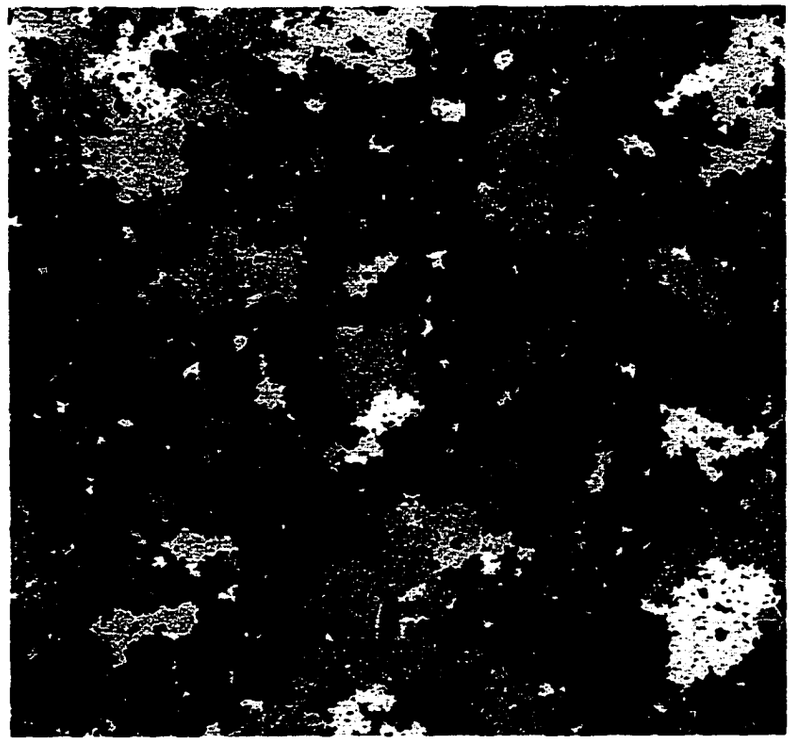

Figure 5.4: A $30,000 \times 30,000$ simulation with disorder $R = 0.65$, where each pixel represents a 30×30 square, and each avalanche is a different color. Note that there are avalanches of all sizes, with many smaller avalanches, and fewer large ones.

a discussion of time and space issues for calculating and storing histograms and correlation functions.

5.1 The Brute Force Method

The brute force method is the easiest one to implement and is competitive for system sizes up to about 10,000 spins. In this method, we store a spin direction and a random field for each site of the lattice. We can then proceed as an experimentalist would by measuring the magnetization at specific predetermined values of H. We start with magnetization $M = -N$ and a large negative field H_0 and then increment to H_1, check all spins in the lattice, and flip those spins in a positive local field. Then we must check the neighbors of the flipped spins again to see if their local fields are now positive. This procedure is continued until all the neighbors of flipped spins have been checked. We then repeat the whole procedure again for a new field H_2, and so on. This approach gives the correct magnetization at the fields H_n: the order in which spins are flipped can be shown not to influence the final state [33, 34, 2]. However, unless the increments in H are very small, several avalanches may occur in a given increment, and all information about single avalanches (such as histograms of avalanche sizes) will be distorted. The time for this method scales as $O(NXT)$, where X is the number of fields H_n at which the magnetization is measured, and T is the average time needed to check the neighbors of the flipped spins measured in units of shells of neighbors.

A variation on this approach is to propagate one avalanche at a time as shown in Fig. 5.5:

use of parallel machines to average over disorder. The fluctuations at the critical point are severe at all system sizes.

1. Find the triggering spin for the next avalanche by checking through the lattice for the unflipped site with the largest internal field $h_i^{\text{int}} = h_i^{\text{eff}} - H$.

2. Increment the external field to just flip that site, and push the spin onto a first-in first-out (FIFO) queue. (see Fig. 5.5, right)

3. Pop the top spin off of the queue.

4. If the spin has not been flipped, flip it and push all unflipped neighbors with positive local fields onto the queue.

5. While there are spins on the queue, repeat from step 3.

6. Repeat from step 1 until all spins are flipped.

This method is standard for avalanche propagation problems. It is also related to the propagation of cluster flips in the Wolff algorithm [35]. Using a queue instead of recursion has two advantages. First, recursion is both slower and more memory intensive, because each recursive call must push all local variables and all registers onto the system stack (which usually has a pre-allocated limit). If we use our own queue, we need only to push the coordinate of the next spin on the queue each time, and we can make the queue as large as necessary. Second, in order to produce a natural spin-flip order, we want to flip all spins that are ready to flip at a given time *before* we flip the spins that they cause to flip. If we put spins that are ready to flip on a FIFO queue, we correctly achieve this order. This procedure corresponds to doing a breadth-first search. Recursion, which is the same as putting the spins on a LIFO stack, would explore all possible consequences of flipping the first neighbor it looks at before it considers the second neighbor. This depth-first search produces an unnatural spin-flip order (although the final state after the avalanche is

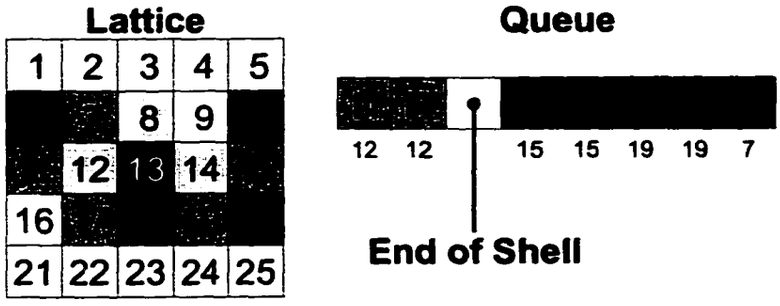

Figure 5.5: Example of how a queue is used to propagate an avalanche. The colored spins are spins which either have flipped in the current avalanche or will flip in the current avalanche. Spin 13 triggered the avalanche, then the light grey spins (14,8,12) were put on the queue as the first shell. As they flipped, the second shell, the blue spins (15,19,7,11,17), were put on the queue. As the first blue spins (15,19,7) flipped, the dark red spins (10,20,20,18,6) were added to the queue as the start of the third shell. The next spin to flip is at the left hand side of the queue. When this spin flips, its neighbors will be checked, and the neighbors that are ready to flip will be added to the right hand side of the queue. The small numbers below the spins in the queue indicate which neighbor caused the spin to be put on the queue. Notice that different neighbors can cause a spin (such as spin 20) to be put on the queue more than once. We have to be careful to only flip the spin once.

unchanged [33, 34, 2]). The dynamics during the avalanche of Fig. 5.2 assumes one shell of spins flipped during each time slice, which is easy to determine by placing markers on a FIFO spin queue, as shown in Fig. 5.5. Each time one pops the marker off of the queue, one starts a new shell and puts the marker back on the end of the queue.

Doing the brute force algorithm one avalanche at a time is very inefficient except at very low disorders. Sweeping through the entire lattice for each avalanche takes $O(N)$ time per avalanche. Since there are $O(N)$ avalanches, the total running time scales as $O(N^2)$. A hybrid approach, finite steps in field followed by internal propagation of avalanches, could be quite efficient if one is solely interested in the magnetization at those fields. A brute force method is probably necessary when simulating systems with dipole-dipole interactions [14].

5.2 Time Efficiency: Sorted Lists

The brute force method is very inefficient at locating the origin of the next avalanche, and one is immediately led to think of storing the several largest local fields in each sweep. If we take this thinking to its logical conclusion, we are led to store a list of all of the spins in the system, sorted according to their random fields.

Unfortunately, life is complicated by the fact that spins experience not only their local random fields, but also fields from their neighbors. To find the origin of the next avalanche, we use the following algorithm:

1. Define an array nextPossible[$n_\uparrow$], $n_\uparrow = 0, 1 \ldots z$, which points to the location in the sorted list of the next spin which would flip if it had $n_\uparrow$ neighbors. Initially, all the elements of nextPossible[$n_\uparrow$] point to the spin with the largest

local random field, h_i.

2. Choose from the $z+1$ spins pointed to by nextPossible, the one with the largest internal field $h_i^{\rm int}[n_\uparrow] = n_\uparrow - n_\downarrow + h_i = 2n_\uparrow - z + h_i$.

3. Move the pointer nextPossible$[n_\uparrow]$ to the next spin on the sorted list.

4. If the spin with the largest $h_i^{\rm int}[n_\uparrow]$ has $n_\uparrow$ up neighbors, then flip it. Otherwise go back to step 2.

An example of the sorted list and the pointers from nextPossible is shown in Fig. 5.6.

The sorting of spins can be done in time $O(N \log N)$. Storage with this algorithm is $N \times$ sizeof(int) for the sorted array (if we reduce the D-dimensional coordinates to one number [6]), and $N \times$ (sizeof(spin) + sizeof(double)) for the lattice itself. Various other compromises between speed of execution and storage are possible, but all leave the running time $O(N \log N)$. The sorted-list algorithm is fast: the largest system sizes we can store on a reasonable workstation execute 1000^2 and 100^3 spins in a few seconds. It is the method of choice for these small systems or when one is interested in the behavior for non-monotonically increasing fields. [7] With some care, the sorted-list algorithm can be extended to work in the presence of infinite range forces.

[6] $(X_1, X_2, \ldots, X_D)$ can be reduced to $X_1 + X_2 L + \cdots + X_D L^{D-1}$. This yields the numbering scheme shown in Figs. 5.5 and 5.6. This reduction also allows us to store a D-dimensional lattice in a one-dimensional array and write code which will work in any number of dimensions.

[7] The sorted-list algorithm can be used for non-monotonically increasing fields with only a few minor additions. When the external field is being lowered instead of raised, the avalanche propagation is the same, except spins are flipped when their local field becomes less than zero instead of when it becomes greater. The nextPossible array needs to be handled carefully. The next spin that would flip up if the field were increased is the last spin that would have already flipped down with the field decreasing. Every time the direction of change of the external field is reversed, all of the nextPossible$[n_\uparrow]$ pointers need to be adjusted by one to account for this.

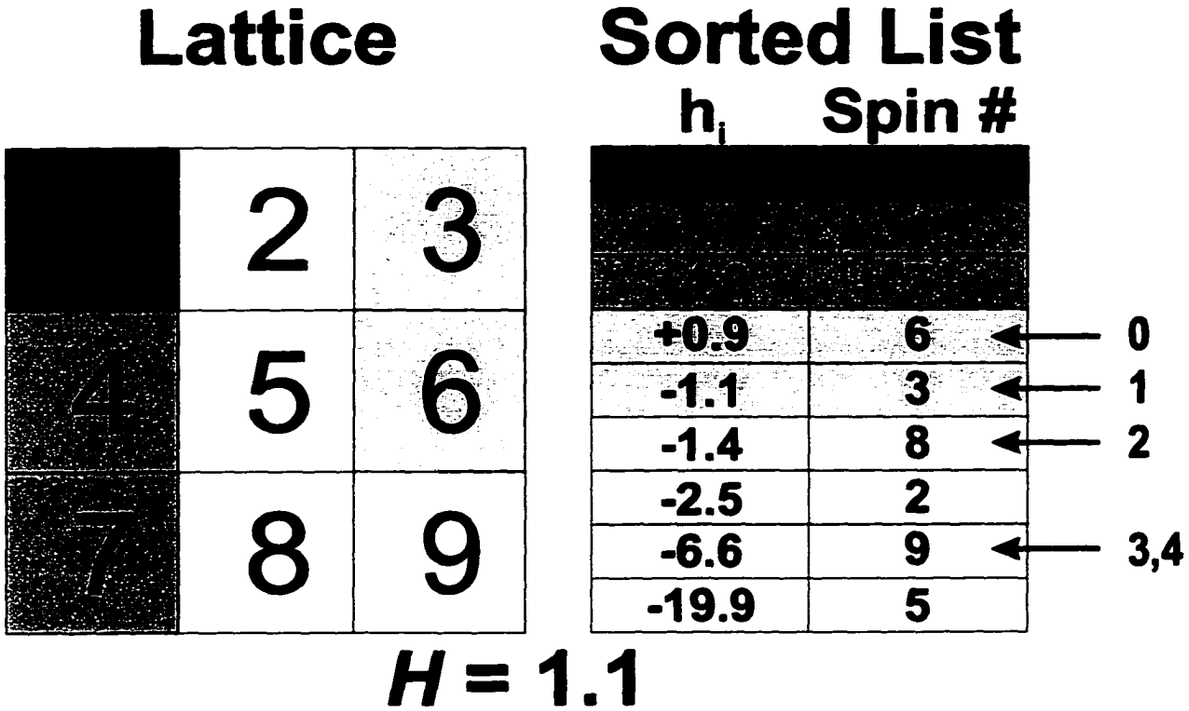

Figure 5.6: Example of how a sorted list is used to find the next spin in the avalanche. The colors indicate spins that have already flipped. The first column in the sorted list contains the random field, and the second column contains the number of the spin with that random field. The arrows to the right indicate the nextPossible[$n_\uparrow$] pointers — the first spin that would not flip with $n_\uparrow$ neighbors up. The spins pointed to are the possible starting locations for the next avalanche. Notice that some of the pointers point to spins that have already flipped. This means that these spins have more than $n_\uparrow$ neighbors up. In a larger system, the unflipped spins will not all be contiguous in the list.

5.3 Space Efficiency: One Bit per Spin

The combination of the rapid execution of the sorted-list algorithm and large finite size effects led us to develop an algorithm optimized for memory efficiency. The key is to recognize that we need never generate the random fields! In invasion percolation [36] (and in the interface problem [7] analogous to ours) one generates the random fields only on sites along the boundary of the growing cluster. In our problem, we can take things further: for each change in a spin's local field given by eq. (5.3), we generate only the probability that it will flip. Storing the random fields is unnecessary because the external field, the configuration of the spin's neighbors, and the knowledge that the spin has not yet flipped gives us all the information which we need to determine the probability that the spin will flip. The only quantity which we must store for each site of the lattice is whether the spin is up or down. Thus, we can store each site of the lattice as a computer bit saving large amounts of memory.

For a monotonically increasing external field, the conditional probability that a spin flips before its non-random local field, $H_{\rm nr} \equiv H + (2n_\uparrow - z)$, reaches $H_{\rm nr} + \Delta H_{\rm nr}$ given that it has not flipped by $H_{\rm nr}$ is

$$P_{\rm flip}(H_{\rm nr}, \Delta H_{\rm nr}) = \frac{(P_\downarrow(H_{\rm nr}) - P_\downarrow(H_{\rm nr} + \Delta H_{\rm nr}))}{P_\downarrow(H_{\rm nr})}, \tag{5.4}$$

where $P_\downarrow(H_{\rm nr})$ is the probability that a spin will point down when the local field is $H_{\rm nr}$. A spin with local field $H_{\rm nr}$ will point down if its random field h_i satisfies $h_i + H_{\rm nr} \leq 0$. This condition implies that the probability that a spin with $n_\uparrow$ up neighbors points down is

$$\begin{aligned} P_\downarrow(n_\uparrow, H) &= \int_{-\infty}^{-H_{\rm nr}(n_\uparrow, H)} \rho(h)\, dh & (5.5) \\ &= \frac{1}{2} + \frac{1}{2}\mathrm{erf}\left(-H_{\rm nr}(n_\uparrow, H)/\sqrt{2}R\right) \\ &= \frac{1}{2}\mathrm{erfc}\left(H_{\rm nr}(n_\uparrow, H)/\sqrt{2}R\right). & (5.6) \end{aligned}$$

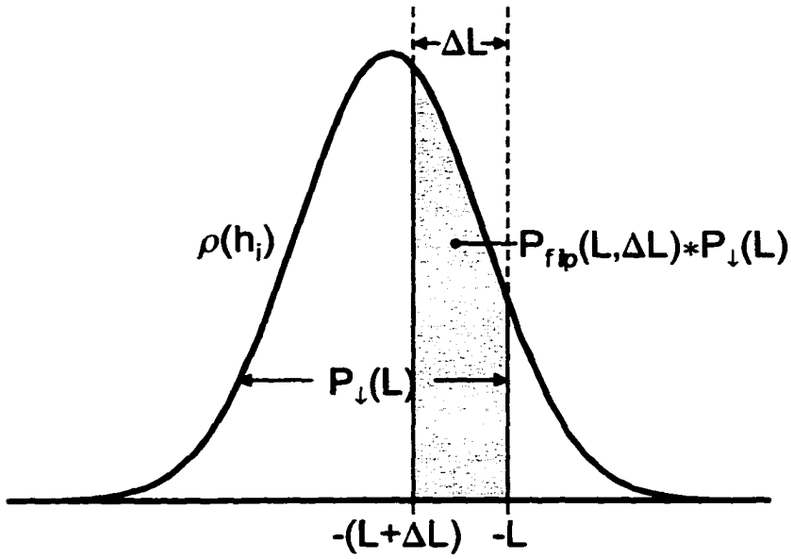

Figure 5.7: The probability that a spin will not have flipped by the time its local field reaches L is the probability that the random field is less than $-L$. This probability is represented by the shaded area of the Gaussian. The probability that the spin will flip before the field reaches $-(L + \Delta L)$ is represented by the area of the darker region divided by the area of the shaded region.

(Writing $P_\downarrow$ in terms of the erfc function cured some problems with rounding at large negative fields H.) These probabilities are illustrated graphically in Fig. 5.7.

Finding the next avalanche is subtle when the random fields are not stored: changing the external field H introduces a probability that any unflipped spin in the lattice may flip. Inspired by the continuous time Monte-Carlo algorithm [37], we keep track of $N_{n_\uparrow}$, the number of down spins which have $n_\uparrow$ up neighbors. Given the probabilities that spins with $n_\uparrow$ up neighbors will flip, we calculate both the change in the external field ΔH needed to flip the next spin and the probability that the next spin to flip has $n_\uparrow$ up neighbors. We then randomly choose $n_\uparrow$, and search at random through the lattice for a spin with $n_\uparrow$ up neighbors. The time taken for the

search is the part of the algorithm which scales worst for large N. If there are $N_{n_\uparrow}$ spins left, this search will take an average time $O(N/N_{n_\uparrow})$. Summing over $N_{n_\uparrow}$ and $n_\uparrow$ yields a bound of order $zN \log N$. In one of our programs, we use a tree structure to do this search more efficiently; this complication decreases the running time by 40% for a 500^2 system at $R = 1$.

How do we calculate ΔH? From eq. (5.4), the probability that a single spin with $n_\uparrow$ neighbors up has not flipped in the range ΔH is $1 - P_{\text{flip}}(n_\uparrow, H, \Delta H) = P_\downarrow(n_\uparrow, H + \Delta H)/P_\downarrow(n_\uparrow, H)$. The probability that no spin with $n_\uparrow$ up neighbors has flipped in this range is

$$P_{n_\uparrow}^{\text{none}} = \left(\frac{P_\downarrow(n_\uparrow, H + \Delta H)}{P_\downarrow(n_\uparrow, H)} \right)^{N_{n_\uparrow}}, \tag{5.7}$$

and the probability that no spin has flipped between H and $H + \Delta H$ is

$$P^{\text{none}}(\Delta H) = \prod_{n_\uparrow=0}^{z} P_{n_\uparrow}^{\text{none}}. \tag{5.8}$$

To find ΔH, we choose a random number r uniformly distributed between zero and one, and set ΔH so that $P^{\text{none}}(\Delta H) = r$.

Unfortunately, we cannot solve for ΔH analytically, and we must find a numerical solution. To find this solution efficiently, we must have a good initial guess. In analogy with nuclear decay, if spins flip with a constant rate Γ, we expect the probability that no spins have yet flipped to be $e^{-\Gamma \Delta H}$. So, for a first approximation of ΔH, we assume that the spin-flip rate Γ is a constant, and therefore

$$\Delta H_1 = -\frac{\log(r)}{\Gamma(H)}. \tag{5.9}$$

where $\Gamma(H)$ is given by

$$\begin{aligned}\Gamma(H) &= -\frac{d\log(P^{\text{none}}(\Delta H=0))}{d\Delta H} \\ &= -\sum_{n_\uparrow=0}^{z} N_{n_\uparrow}\frac{d\log(P_\downarrow(n_\uparrow,H+\Delta H))}{d\Delta H} \\ &= \sum_{n_\uparrow=0}^{z} N_{n_\uparrow}\frac{\rho(H_{\text{nr}}(n_\uparrow,H))}{P_\downarrow(n_\uparrow,H)} \\ &\equiv \sum_{n_\uparrow=0}^{z}\Gamma(n_\uparrow,H) \qquad (5.10)\end{aligned}$$

We can make a better second guess by looking at the error in our first guess. If the error in our guess is $\Delta r = P^{\text{none}}(\Delta H) - r$, then we can make an improved second guess for ΔH by aiming for $r - \Delta r$:

$$\Delta H_2 = -\frac{\log(r-\Delta r)}{\Gamma(H)}. \qquad (5.11)$$

These two guesses can then be used as input into a root finding routine [8]. Note that while these guesses are usually very good for small $|H|$ and lead to quick solutions, they can be very bad for large $|H|$. If the guesses for ΔH are very large, it may be better to choose two arbitrary guesses. In our code, if $\Delta H_1 > 20$, we use $\Delta H_1 = 0$ and $\Delta H_2 = 20$ for the two guesses.

Our algorithm for finding the next avalanche becomes

1. Choose a random number r uniformly distributed between zero and one.

2. Pre-calculate the values of $P_\downarrow(n_\uparrow, H)$. These values will be used repeatedly in solving for ΔH.

[8] We use a simple algorithm to make sure that the guesses are on opposite sides of the correct guess, and then use the Brent algorithm to find the root. The Brent algorithm uses a combination of interpolation when the guesses are close, and bisection when the interpolation works badly. Descriptions and implementations of this and other root finding algorithms can be found in Refs. [38] and [39].

3. Calculate guesses for ΔH using eqs. (5.9) and (5.11) and use them as input to a root finding routine to find the exact solution for ΔH.

4. Increment H by ΔH.

5. Calculate the array probFlip[$n_\uparrow$] for use in the remainder of the avalanche, where probFlip[$n_\uparrow$] is the probability at the current field H that a spin will flip when its number of up neighbors changes from $n_\uparrow$ to $n_\uparrow$+1 (see eq. (5.4)).

6. Calculate the rates for flipping spins for each $n_\uparrow$ *at the current field* $H = H_{\text{old}} + \Delta H$:

$$\Gamma(n_\uparrow, H) = N_{n_\uparrow} \rho(H_{\text{nr}}(n_\uparrow, H))/P_\downarrow(n_\uparrow, H) \tag{5.12}$$

and the total rate $\Gamma(H) = \sum_{n_\uparrow=0}^{z} \Gamma(n_\uparrow, H)$.

7. Choose a random number uniformly distributed between zero and Γ and use it to select $n_\uparrow$.

8. Search at random in the lattice for an unflipped spin with $n_\uparrow$ up neighbors [9].

9. Start the avalanche at that spin. During an avalanche, the algorithm is essentially the same as the brute force algorithm:

10. Push the first spin onto the queue.

11. Pop the top spin off of the queue.

[9] If your random number generator is not good enough, or if you have incorrectly kept track of the number of down spins with $n_\uparrow$ neighbors up, your simulation may enter an infinite loop searching for the next spin. Also, if you are storing your spins in a 1D array, you should still generate D random numbers, one for each coordinate. If you try to save time and only generate one random number, then for a very large system there will be gaps in the random numbers, and some spins will never be found, causing an infinite loop.

12. If the spin is unflipped, flip it, find $n_\uparrow$, and decrease $N_{n_\uparrow}$ by one. Otherwise, skip to step 14.

13. Look at all unflipped neighbors. For each unflipped neighbor, find the current number of up neighbors, $n_\uparrow$; decrease $N_{n_\uparrow - 1}$ by one, and increase $N_{n_\uparrow}$ by one. Push the spin on the queue [10] with probability probFlip$[n_\uparrow - 1]$, as calculated in step (5).

14. While there are spins left in the queue, repeat from step 11.

15. While there are unflipped spins, repeat from step 1.

This algorithm is about half as fast in practice as the sorted-list algorithm which is faster than we expected. The overhead involved in solving for ΔH is presumably compensated by the time saved not shifting data in and out of cache. Systems of 10^9 spins take a few days of CPU time on a reasonable workstation; $30,000^2$ systems take less than 15 hours on a 266 MHz Pentium II.

5.4 Calculating Histograms and Correlations

Several functions are needed to characterize the critical properties of our model. The simplest function is the magnetization M as a function of the external field H. We also calculate distributions of avalanche sizes (Fig. 5.3, top), and correlation functions. Some care must be taken to make sure that the calculation of these

[10] One might worry that the queue will grow very large. However, the queue will only be as large as the largest shell of spins, which should scale as the surface area of the largest avalanche. Therefore, it should scale as $N^{1/2}$ in two dimensions, and as $N^{2/3}$ in three dimensions. Because the avalanches tend to grow in fits and starts, this situation is even better. Notice that in Fig. 5.1, even though the avalanche contained almost 300,000 spins, and the surface area was very large, the largest shell had only 321 spins in it (Fig. 5.2). The queue is generally very small compared with the system size.

functions does not dramatically increase the running time or memory requirements of the simulation.

When doing calculations with a billion spins, one cannot calculate *any* quantity which scales linearly with the system size. Instead of computing $H(M)$ at each avalanche (one GB of data), we are forced to compute $H(M_n)$ at pre-chosen points.

The characteristic feature of the critical point is the appearance of an infinite avalanche. The equivalent of an infinite avalanche in a finite system is an avalanche that spans the entire system in at least one dimension. To tell whether we are above or below the critical point, we need to detect these spanning avalanches. In three and higher dimensions, the number of spanning avalanches as a function of R is also interesting to study. The most obvious way of detecting spanning avalanches is to mark each row as a spin flips in it, and check at the end of the avalanche to see if all the rows contain flipped spins from the avalanche. However, this method requires $O(N^{1/D})$ operations per avalanche. Because there are many small avalanches, this method is unacceptable. A preferable method is to keep track of the $2\times D$ boundaries of the avalanche as it grows. If a pair of boundaries meet, then the avalanche is a spanning avalanche. One must take care to deal properly with the periodic boundary conditions.

Another useful function is the avalanche size distribution $D(S)$, defined as the number of avalanches which flip S spins during the simulation, divided by the total number of spins. Like the $M(H)$ curve, the avalanche size distribution scales linearly with the system size. Thus, we need bins up to size N, the size of the largest possible avalanche. Logarithmic binning is the obvious solution, with bin n including all sizes $b_a^{n-1} < S < b_a^n$. We have chosen b_a from 1.01 to 1.1. Large bins are preferable for lower statistical noise. This choice is particularly important in the tail of very large

avalanches, where small bins would contain few avalanches. However, very large bins will systematically alter the shape of the scaling functions (although they will not change the critical exponents). It is important to divide the final population in each bin by the number of integers contained within the bin (and not just the bin width). Clearly one should also ignore the early bins which do not contain any integers.

We calculate the correlation function $G(x, R)$ within an avalanche, where $G(x, R)$ gives the probability that the first spin in an avalanche will cause a spin a distance x away to flip in the same avalanche. At the beginning of each avalanche, we record the coordinates of the first spin in the avalanche. Then, for each subsequent spin in the avalanche, we calculate the distance x to the first spin, and add one to the appropriate bin. Logarithmic binning is not necessary for the correlation function, because the size of the correlation function is proportional to the length of the system, not the total number of spins. Thus, we use a fixed bin size $b_c = 1$. At the end of the simulation, each bin should be normalized by the number of spins which are between $x - b_c/2$ and $x + b_c/2$ away from the origin.

The only tricky part of calculating $G(x, R)$ comes from the periodic boundary conditions. If the avalanche crosses a boundary, two points at opposite ends of the avalanche can come close together. Because we do not calculate $G(x, R)$ for spanning avalanches, we know that there will be at least one row in every dimension which is not touched by the avalanche. To calculate separations, we use the periodicity of the lattice and the continuity of the avalanche to shift the coordinates so they are all on one side of these empty rows. Because we are already keeping track of the boundaries of the avalanche for the detection of spanning avalanches, finding an empty row is easy.

The running times of the three algorithms as a function of system size are shown in Fig. 5.8. The brute force algorithm can be useful when one cares only about $M(H)$ at a few points, but is otherwise too slow to implement large systems. The sorted-list algorithm is the fastest algorithm, but on a 128 MB machine, only system sizes of about six million spins can be run. The bits algorithm is almost as fast as the sorted-list algorithm, and asymptotically uses only one bit of memory per spin.

Note that all three algorithms are limited to 2,147,483,648 spins unless more sophisticated data structures are used to hold the spins—the long integers which are used to index the spin arrays cannot hold a number larger than 2,147,483,648.

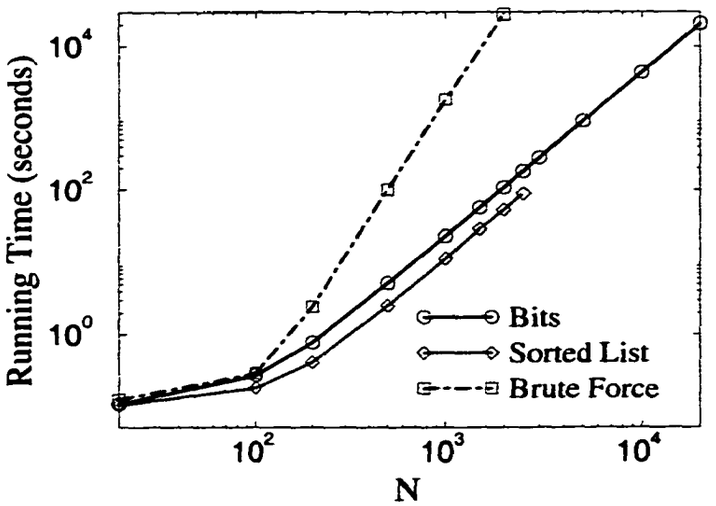

Figure 5.8: The running times for the three algorithms for two-dimensional systems with $R = 1.0$ on a 266 MHz Pentium II with 128 MB of memory. Note that both the bits algorithm and the sorted-list algorithm have run times which grow approximately linearly (the $\log N$ is not visible), and the brute force running time grows quadratically. Also notice that the largest bits simulation was 64 times larger than the largest sorted-list simulation.

Appendix A

The mean field power spectrum

In mean field theory, we can calculate the power spectrum exactly. The Hamiltonian in mean field theory is the Hamiltonian in equation 2.2, without nearest neighbor or dipole terms:

$$\mathcal{H} = -\sum_i (H + J + h_i)s_i. \tag{A.1}$$

When a spin flips with an external field of H, all spins with random fields between $-(H+JM)$ and $-(H+J(M+2/N))$ will flip. Therefore, each spin has a probability of $\frac{2J}{N}\rho(-H - JM)$ of flipping, where $\rho(h)$ is the probability distribution of the random fields. On average, $2J\rho(-H - JM)$ spins will be flipped. If $2J\rho(-H - JM) > 1$, then the avalanche will tend to grow indefinitely, and there will be an infinite avalanche. If $2J\rho(-H - JM) < 1$, then the avalanche will quickly die out, and all avalanches will be small. If $2J\rho(-H - JM) = 1$, then avalanches will always be finely balanced between continuing and dying, and there will be a critical distribution of avalanches. If the random field distribution $\rho(h)$ has a maximum value of $1/2J$, then there will be a critical distribution of avalanches at the value of $H = H_c$ where $\rho(h)$ is a maximum.

Let us calculate the power spectrum for the critical system with $\rho(h) = 1/2J$. To begin with, we will calculate the probability distribution of time-series $n_1, n_2, \ldots, n_\infty$. We know that in shell zero, exactly $n_0 = 1$ spins will flip. At the critical point, where each spin on average causes one more spin to flip, shell one will have a Poisson distribution with mean one: $P(n_1) = \frac{1}{en_1!}$. Shell i will have a Poisson distribution with mean n_{i-1}: $P(n_i) = \frac{e^{n_i-1}n_{i-1}^{n_i}}{n_i!}$. Therefore, the probability distribution for the entire time series will be

$$P(1, n_1, n_2, \ldots, n_\infty) = \frac{1}{en_1!}\prod_{i=2}^{\infty}\frac{e^{n_i-1}n_{i-1}^{n_i}}{n_i!}. \tag{A.2}$$

Now, from equation A.2, we can calculate the average time-time correlation function

$$G(\theta) = \sum_{i=0}^{\infty}\langle n_i n_{i+\theta}\rangle, \tag{A.3}$$

where

$$\langle n_i n_{i+\theta}\rangle = \sum_{\{n1,\ldots,n_\infty\}=0} n_i n_{i+\theta} P(n_1, \ldots, n_\infty). \tag{A.4}$$

To simplify equation A.4, we need to use several properties of the Poisson distribution: $\sum_{n=0}^{\infty}\frac{e^{-x}x^n}{n!} = 1$, $\sum_{n=0}^{\infty} n\frac{e^{-x}x^n}{n!} = x$, and $\sum_{n=0}^{\infty} n^2\frac{e^{-x}x^n}{n!} = x + x^2$. Using the first rule repeatedly, we can simplify equation A.4 to

$$\langle n_i n_{i+\theta}\rangle = \sum_{\{n_1,\ldots,n_{i+\theta}\}=0}^{\infty} n_i n_{i+\theta} P(n_1, \ldots, n_{i+\theta}).$$

Then, using the second rule repeatedly, we can further simplify to

$$\langle n_i n_{i+\theta}\rangle = \sum_{\{n_1,\ldots,n_i\}=0}^{\infty} n_i^2 P(n_1, \ldots, n_i).$$

Now, applying the second and third rules repeatedly, we can simplify to a single

sum:

$$\langle n_i n_{i+\theta} \rangle = \sum_{n_1=0}^{\infty} \frac{(i-1)n_1 + n_1^2}{e n_1!}$$
$$= i + 1. \tag{A.5}$$

Notice that the correlation between two times is proportional only to the first time, and not the separation between the times.

Now, we can find the value of the time-time correlation function $G(\theta)$ by summing the result of equation A.5. Because the time-time correlation function as defined is proportional to the square of the total time, we must cut off the summation at some maximum time T to get a finite result. Summing according to equation A.3, we find

$$\begin{aligned} G(\theta) &= \sum_{i=0}^{T-\theta-1} i + 1 \\ &= \frac{(T-\theta)(T-\theta+1)}{2} \\ &= \frac{T^2}{2} + \frac{T}{2} + \frac{\theta^2}{2} - \frac{\theta}{2} - T\theta. \end{aligned} \tag{A.6}$$

This shape for a cutoff time of $T = 1000$ is shown in figure A.1. Notice that the exact shape in mean-field theory is very similar to the experimentally measured correlation functions in three dimensions.

To get the exact form of the mean-field energy spectrum, we just take the cosine transform of equation A.6.

$$\begin{aligned} E(\omega) &= \int_0^{\infty} \cos(\omega\theta) G(\theta) d\theta \\ &= \int_0^{\infty} \cos(\omega\theta) \left(\frac{T^2}{2} + \frac{T}{2} + \frac{\theta^2}{2} - \frac{\theta}{2} - T\theta \right) d\theta \\ &= T\omega^{-2} + \frac{\omega^{-2}}{2}(1 - \cos(T\omega)) - \omega^{-3}\sin(T\omega). \end{aligned} \tag{A.7}$$

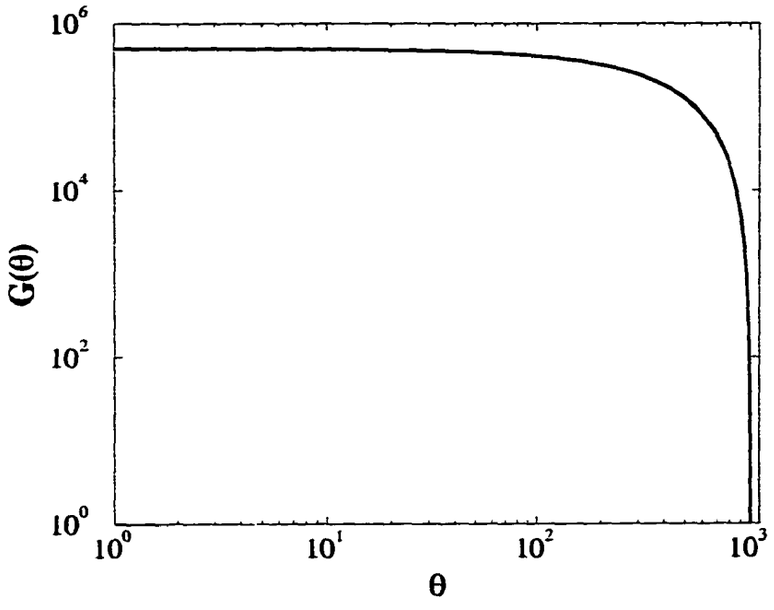

Figure A.1: The exact time-time correlation for mean field theory with a maximum time cutoff of $T = 1000$.

The dominant term in this equation is $T\omega^{-2}$. This is the same exponent as predicted by the general scaling arguments: $\frac{1}{\sigma\nu z} = 2$. The general scaling arguments also predicted that a term smaller by a factor of T and with the exponent $(3-\tau)/\sigma\nu z = 3$ would be subtracted off, and it is, but multiplied by a factor of $\sin(T\omega)$. However, the $\sin(T\omega)$ turns out to simplify things even more. Because the correlation function was actually discrete, we should consider a discrete power spectrum, where the frequencies are multiples of $\omega_0 = \frac{2\pi}{T}$. This means that $\cos(T\omega) = 1$ and $\sin(T\omega) = 0$ for all ω in the discrete spectrum. Because of this, all terms except the $T\omega^{-2}$ term drop out. If we divide by T to get the power spectrum, we find

$$\mathcal{P}(\omega) = \omega^{-2}. \tag{A.8}$$

Bibliography

[1] B. Allesandro, C. Beatrice, G. Bertotti, and A. Montorsi, J. Appl. Phys. **68**(6), 2901 (September 1990).

[2] J. P. Sethna, K. Dahmen, S. Kartha, J. A. Krumhansl, B. W. Roberts, and J. D. Shore, Phys. Rev. Lett. **70**(21), 3347 (May 1993).

[3] K. Dahmen, S. Kartha, J. A. Krumhansl, B. W. Roberts, J. P. Sethna, and J. D. Shore, J. Appl. Phys **75**(10), 5946 (May 1994).

[4] O. Perković, K. Dahmen, and J. P. Sethna, Phys. Rev. Lett. **75**(24), 4528 (December 1995).

[5] O. Perković, K. A. Dahmen, and J. P. Sethna, *Disorder-induced critical phenomena in hysteresis: Numerical scaling in three and higher dimensions*, cond-mat #9807336, Los Alamos Nat'l Laboratory, Los Alamos, N. M.; http://xxx.lanl.gov/abs/cond-mat/9807336.

[6] K. A. Dahmen and J. P. Sethna, Phys. Rev. B. **53**(22), 14872 (June 1996).

[7] H. Ji and M. O. Robbins, Phys. Rev. B **46**(22). 14519 (1 December 1992).

[8] P. Cizeau, S. Zapperi, G. Durin, and H. E. Stanley, Phys. Rev. Lett. **79**(23), 4669 (December 1997).

[9] O. Narayan, Phys. Rev. Lett. **77**(18), 3855 (October 1996).

[10] J. S. Urbach, R. C. Madison, and J. T. Markert, Phys. Rev. Lett. **75**(2), 276 (July 1995).

[11] K. A. Dahmen, *Hysteresis, Avalanhces, and Disorder Induced Critical Scaling: A Renormalization Group Approach*, Ph.D. thesis, Cornell University (May 1995).

[12] D. Spasojević, S. Bukvić, S. Milosević, and H. E. Stanley, Physical Review E **54**(3), 2531 (September 1996).

[13] H. J. Jensen, K. Christensen, and H. C. Fogedby, Phys. Rev. B **40**(10), 7425 (October 1 1989).

[14] S. Zapperi, P. Cizeau, G. Durin, and H. E. Stanley, Physical Review B **58**(10) (September 1998).

[15] W. Grosse-Nobis, Journal of Magnetism and Magnetic Materials **4**, 247 (1977).

[16] G. Durin and S. Zapperi, Journal of Applied Physics **85**(8), 5196 (April 1999).

[17] B. Alessandro, C. Beatrice, G. Bertotti, and A. Montorsi, J. Appl. Phys. **68**(6), 2908 (September 1990).

[18] G. Bertotti, G. Durin, and A. Magni, J. Appl. Phys. **75**(10), 5490 (May 1994).

[19] U. Lieneweg and W. Grosse-Nobis, Intern. J. Magnetism **3**, 11 (1972).

[20] P. J. Cote and L. V. Meisel, Phys. Rev. Lett. **67**(10), 1334 (Sept 1991).

[21] L. V. Meisel and P. J. Cote, Phys. Rev. B **46**(17), 10822 (Nov 1992).

[22] G. Bertotti, F. Fiorillo, and A. Montorsi, J. Appl. Phys. **67**(9), 5574 (May 1990).

[23] P. Bak, C. Tang, and K. Wiesenfeld, Phys. Rev. A **38**(1), 364 (July 1 1998).

[24] A. J. Bray and M. A. Moore, Journal of Physics C **18** (1985).

[25] B. Drossel and K. Dahmen, Eur. Phys. J. B **3** (1998).

[26] P. W. Anderson, D. J. Thouless, E. Abrahams, and D. S. Fisher, Phys. rev. B **22**(8), 3519 (1980).

[27] D. S. Fisher and A. P. Young, Phys. rev. B **58**(14), 9131 (1998).

[28] D. S. Fisher, Phys. rev. lett. **69**(3), 534 (1992).

[29] D. S. Fisher, Phys. rev. B **51**(10), 6411 (1995).

[30] E. Vives, J. Goicoechea, J. Ortin, and A. Planes, Phys. Rev. E **52** (1995), vives *et al.* studied random-field random-bond systems up to 100×100. Our methods are not directly applicable to random bond systems or to systems with long-range forces [14].

[31] R. Blossey, T. Kinoshita, and J. Dupont-Roc, Physica A **248** (1998), blossey *et al.* studied the prewetting transition with our model using the efficient form of the brute force algorithm, on systems up to 900×900.

[32] J. P. Sethna, O. Perković, and K. A. Dahmen, in B. Dubrulle, F. Graner, and D. Sornette, eds., *Scale Invariance and Beyond, Les Houches Workshop* (Springer, Berlin), Les Houches Workshop, p. 87. Figure 1 (right) is incorrect in this reference: it shows dM/dt for the whole hysteresis loop, not just one avalanche.

[33] A. A. Middleton, Phys. Rev. Lett. **68** (1992).

[34] A. A. Middleton and D. S. Fisher, Phys. Rev. B **47** (1993).

[35] U. Wolff, Phys. Rev. Lett. **62** (1989).

[36] L. Furuberg, J. Feder, A. Aharony, and T. Jøssang, Phys. Rev. Lett. **61** (1988).

[37] A. B. B. M. H. Kalos and J. L. Leibowitz, J. Comp. Phys. **17** (1975).

[38] W. H. Press, S. A. Teukolsky, and W. T. Vetterling, *Numerical Recipes in C: The Art of Scientific Computing* (Cambridge University Press, 1992), the book is also available online at http://www.nr.com/.

[39] NetLib is a collection of mathematical software, papers and databases at http://www.netlib.org/.

[40] O. Narayan and D. S. Fisher, Phys. Rev. B **48**(10), 7030 (September 1993).

[41] F. Pázmándi, G. Zaránd, and G. T. Zimányi, cond-mat/9902156 (February 1999).

[42] B. Tadić and U. Nowak, cond-mat/9903090 (March 1999).

[43] A. Vásquez and O. Sotolongo-Costa, cond-mat/9903207 (March 1999).

[44] E. Obradó, E. Vives, and A. Planes, Physical Review B **59**(21) (June 1999).

[45] S. Field, J. Witt, F. Nori, and X. Ling, Phys. Rev. Lett. **74**(7), 1206 (February 13 1995).

[46] E. Vives, J. Ortín, L. Mañoso, I. Ràfols, and R. Pérez-Magrané, Phys. Rev. Lett. **72**(11), 1694 (March 14 1994).